MICROCOPY RESOLUTION TEST CHART

AFWAL-TR-81-2088

OPTICAL HETERODYNE STRAIN SENSOR

UNITED TECHNOLOGIES RESEARCH CENTER
OPTICS & ACOUSTICS GROUP
EAST HARTFORD, CONNECTICUT 06108

DTIC
ELECTED
S FEB 1 1982
B

SEPTEMBER 1981

Final Report for Period September 1980 to August 1981

AERO PROPULSION LABORATORY
AIR FORCE WRIGHT AERONAUTICAL LABORATORIES
AIR FORCE SYSTEMS COMMAND
WRIGHT-PATTERSON AIR FORCE BASE, OHIO 45433

82 02 01 165

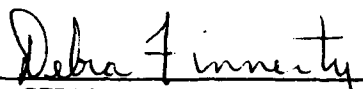This technical report has been reviewed and is approved for publication.

DEBRA FINNERTY
Project Engineer

ISAK J. GERSHON
Technical Area Manager
Mechanical Design Group

FOR THE COMMANDER

JAMES M. SHIPMAN, Maj, USAF
Chief, Components Branch

REPORT DOCUMENTATION PAGE		READ INSTRUCTIONS BEFORE COMPLETING FORM
1. REPORT NUMBER AFWAL-TR-81-2088	2. GOVT ACCESSION NO. AD-A110288	3. RECIPIENT'S CATALOG NUMBER
4. TITLE (and Subtitle) OPTICAL HETERODYNE STRAIN SENSOR		5. TYPE OF REPORT & PERIOD COVERED FINAL Sep 80 – Aug 81
		6. PERFORMING ORG. REPORT NUMBER R81-995310
7. AUTHOR(s) Karl A. Stetson Robert K. Erf		8. CONTRACT OR GRANT NUMBER(s) F33615-80-C-2067
9. PERFORMING ORGANIZATION NAME AND ADDRESS United Technologies Research Center Optics & Acoustics Group East Hartford, CT 06108		10. PROGRAM ELEMENT, PROJECT, TASK AREA & WORK UNIT NUMBERS 62203F 3066 12 65
11. CONTROLLING OFFICE NAME AND ADDRESS Aero Propulsion Laboratory (AFWAL/POTC) AF Wright Aeronautical Laboratories, AFSC Wright-Patterson AFB, OH 45433		12. REPORT DATE September 1981
		13. NUMBER OF PAGES 86
14. MONITORING AGENCY NAME & ADDRESS(if different from Controlling Office)		15. SECURITY CLASS. (of this report) Unclassified
		15a. DECLASSIFICATION/DOWNGRADING SCHEDULE

16. DISTRIBUTION STATEMENT (of this Report)

Approved for Public Release; distribution unlimited.

17. DISTRIBUTION STATEMENT (of the abstract entered in Block 20, if different from Report)

18. SUPPLEMENTARY NOTES

19. KEY WORDS (Continue on reverse side if necessary and identify by block number)

Static Strain Gage, Dynamic Strain Gage, Heterodyne Interferometry,
Optical Strain Sensor, Crack Detection.

20. ABSTRACT (Continue on reverse side if necessary and identify by block number)

It has been demonstrated that heterodyne optical strain sensing can be used to measure both static and vibratory strains to a range of 2000 microstrain with a sensitivity approaching one microstrain and an accuracy approaching one percent. The theoretical and experimental work undertaken to develop a heterodyne optical strain sensing system, as described herein, includes: 1) the fabrication of a prototype device; 2) a system evaluation study; and 3) application to a beam, turbine blade and crack detection. In addition to a detailed discussion of the results, the principles of heterodyne optical strain measurements,

DD FORM 1473 EDITION OF 1 NOV 65 IS OBSOLETE

as originally conceived at the United Technologies Research Center, are presented

SUMMARY

It has been demonstrated that heterodyne optical strain sensing can be
used to measure both static and vibratory strains to a range of 2000 microstrain
with a sensitivity approaching one microstrain and an accuracy approaching one
percent. Thus, the non-contact measurement of strain with an accuracy comparable
to that of a properly bonded strain gage is feasible and, as such, holds extra-
ordinary potential for the future of strain measurement. Although the system
performance is limited at present by object translations and rotations, which a
strain gage is not, they manifest themselves as a loss in signal, analogous to
faulty bonding of a strain gage, which is a clear indication that the motion has
occurred. Further, insensitivity to object translation can be achieved by proper
spacing between the transform lenses and the recording plane, which is an initial
adjustment that could be preset. With respect to data acquisition, the optical
strain sensor is more rapid than a strain gage, even with conventional photographic
processing. This is a result of the long curing times required for strain gage
adhesives if they are to accurately transmit force from the object surface to the
gage.

The theoretical and experimental work undertaken to develop a heterodyne
optical strain sensing system, as described herein, included: 1) the fabrication
of a prototype device; 2) a system evaluation study; and 3) application to a
beam, turbine blade and crack detection. In addition to a detailed discussion of
the results, the principles of heterodyne optical strain measurement, as originally
conceived at the United Technologies Research Center, are presented. Finally,
additional studies are recommended for the further development of optical strain
measurement techniques to provide for the real-time strain mapping of an object
with immunity to surface rotations.

TABLE OF CONTENTS

LIST OF ILLUSTRATIONS

SECTION I

INTRODUCTION

Most industrial measurements of strain are made with electrical strain gages. Whereas these gages have a good history of reliability, accuracy and convenience, they have, nonetheless, a number of disadvantages. They must be bonded well to the surface of the test object or else they do not give accurate measurement. It is easy for their fine electrical structures to become damaged by mechanical contacts, and they are intrinsically temperature sensitive. For situations where a large number of parts require strain gaging on a routine basis, the use of electrical gages involves considerable time and expense.

Because of these problems associated with electrical strain gages, consider-able effort has been put forth to develop optical methods as alternatives. An optical strain sensor that performs the same function as a strain gage could offer significant advantages even if its sensitivity and accuracy were only comparable. An optical system that measures motions of an object surface directly does not suffer from potential errors due to faulty glue layers or erroneous behavior of a carrier matrix. Furthermore, the speed with which an optical system may be reset to observe a new object location may be quite rapid in the absence of a curing time for an adhesive. However, to date, no truly satisfactory optical method of strain measurement had been developed because of the problems associated with low accuracy, impractically large gage lengths, cumbersome data extraction and pro-cessing requirements, and difficulties dealing with systems that record images, such as hologram interferometry or speckle photography. Although, by these methods, strain information could be recorded at once over an entire object sur-face; in practice, the images must be scanned to generate data for strain analysis.

In response to the need for a solution to the problem of optical strain measurement, UTRC conceived a system (Ref. 1) that operated by means of coherent illumination of two nearby points on an object surface. Preliminary experiments confirmed that surface strains could be extracted in an easy, straightforward manner from the Fourier transform of the field scattered from two such illuminated points. From this starting point, it was possible to envision an optical system for strain measurement that would obtain high accuracy and rapid readout by means of optical heterodyne techniques.

Optical heterodyning is a technique for converting, into electronic form, the pictorial data commonly generated by an interferometer. The bright and dark bands of light that are visible as fringes in the output of an interferometer connect regions of constant optical phase difference between two otherwise identical optical fields. If a constantly changing phase is introduced between the two fields, the resulting fringes scan across the output plane. A stationary detector in that plane will generate an electronic signal whose phase will be

1

directly related to the optical phase difference of the interfering fields. This
is a practical conversion because highly accurate electronic phase meters are
available that can determine electronic phase to within 0.1°. Such an accuracy
corresponds to locating the center of a fringe to within 1/3600 of a fringe
spacing. Equally as important, optical heterodyning makes acquisition of data
possible anywhere in the output plane, thereby obviating the need for fringe-order
interpolation. Furthermore, the data is available in a form that is easily
transmitted to computers or alternative data processing systems.

Because of the connection between optical phase and path length difference,
interferometers are often used for the precise measurement of mechanical displace-
ment. For measurement of strain over short gage lengths, however, the required
displacement measurement accuracy becomes quite severe. Strain may be defined as
the change of length of an object segment divided by the length of the segment
itself. Consequently, for a segment length (defined herein as gage length) of 1
mm, the change in length corresponding to one microstrain (i.e., 10^{-6}) would be
1 nanometer (i.e., 10^{-9} meters). In terms of the visible optical spectrum
(wavelengths of 0.4 to 0.7 micrometers), 1 nanometer is a small fraction of a
fringe order. It is natural, therefore, that the optical heterodyning technique
should be of great help in the interferometric measurement of strain from either
holograms (Ref. 2) or specklegrams (Ref. 3). Consequently, the present study was
undertaken to: 1) fabricate a prototype device of a heterodyne optical strain
sensor (HOSS); 2) evaluate the range, accuracy, and limitations of the method;
and 3) experimentally measure strain on a beam subject to four-point bending, a
turbine engine blade, and across a crack to determine its applicability to crack
detection in metals.

Supported under Contract F33615-80-C-2067, sponsored by the Aero Propulsion
Laboratory, at the Air Force Wright Aeronautical Laboratories, the program
successfully demonstrated that heterodyne optical strain sensing could be used to
measure both static and vibratory strains to a range of 2000 microstrain with a
sensitivity approaching one microstrain and an accuracy approaching one percent.
Presented in the following sections are: an overview of the principles of heter-
odyne optical strain measurement including discussions of the UTRC system concept
and heterodyne interferometry (Section II); a description of the experimental
HOSS system designed, fabricated, and assembled under the contract (Section III);
the procedures employed in the strain measurement calculation for both the static
and vibratory cases (Section IV); a presentation of the analytical investigations
concerned with accuracy, measurement range, object translation, surface tilt, and
system limitations (Section V); the results of the experimental investigations
to measure strains on both a beam and turbine blade, and to examine crack detection
in metals (Section VI); and an enumeration of the significant conclusions of the
study, together with consideration of potential benefits to be derived from
continued development of optical strain sensing techniques (Section VII).

2

SECTION II

PRINCIPLES OF HETERODYNE OPTICAL STRAIN MEASUREMENT

Opto-Mechanical System Configuration

The concept of the UTRC Heterodyne Optical Strain Sensor (HOSS) can be explained by means of Fig. 1. Two narrow light beams are obtained from a laser and directed by a small mirror, M, so as to illuminate two nearby points on an object, A and B. The surface, being rough, will scatter light in wide, conical angles from its illuminated regions. A lens is placed at a distance of one focal length away from the object surface so that it collimates the fields scattered from each point. At a distance of one focal length on the other side of the lens, a recording is made of the interference pattern that results from the coherent addition of the two fields. (The field at this recording plane is the optical Fourier transform of the field at the object surface.) The field from each illuminated point will be speckled due to the random scattering within each illuminated region on the object. Because of the lateral separation of the two points, the two fields at the transform plane will be inclined at an angle to one another, causing a fine interference pattern to appear where the speckles of the two fields overlap. Such a pattern is shown in Fig. 2.

If, after it has been developed, the recording is relocated in the same position it occupied during exposure, a black-silver image will occupy the illuminated areas, while the transparent portions of the recording will not be illuminated. This will result in a minimum of light transmitted through the recording. If the phase of the illuminating beams are shifted by 180° relative to one another, the fine interference pattern will shift by one-half cycle relative to the recording at the transform plane. The transparent areas of the recording will now be illuminated, and this will result in a maximum of light being transmitted through the recording. This beating of a pattern of illumination with its photographic replica is often referred to as moiré interference.

Moiré interference at the transform plane of the system illustrated in Fig. 1 can be used effectively to measure strain on an object surface. If the object surface is strained so that points A and B increase their separation, the angle between the two fields at the transform plane will increase. This, in turn, will increase the spatial frequency of the fine interference fringes relative to the recording. If this frequency increase is small relative to the spatial frequency itself, its effect will be to generate a spatially cyclic change of phase between the two patterns, which will cause a spatially cyclic fluctuation of light transmitted through the recording. This will appear to the observer as a fringe pattern, an example of which is shown in Fig. 3. The spatial frequency of the moiré fringe pattern in the ω_x direction is proportional to the x strain.

FIG. 1

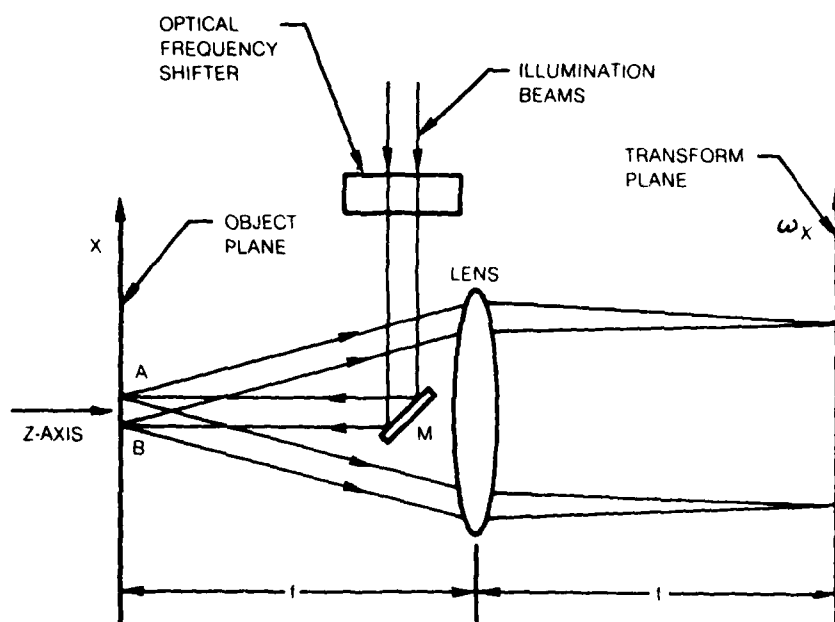## OPTICAL STRAIN SENSOR CONCEPT

4

FIG. 2

INTERFERENCE OF TWO INCLINED SPECKLE FIELDS

FIG. 3
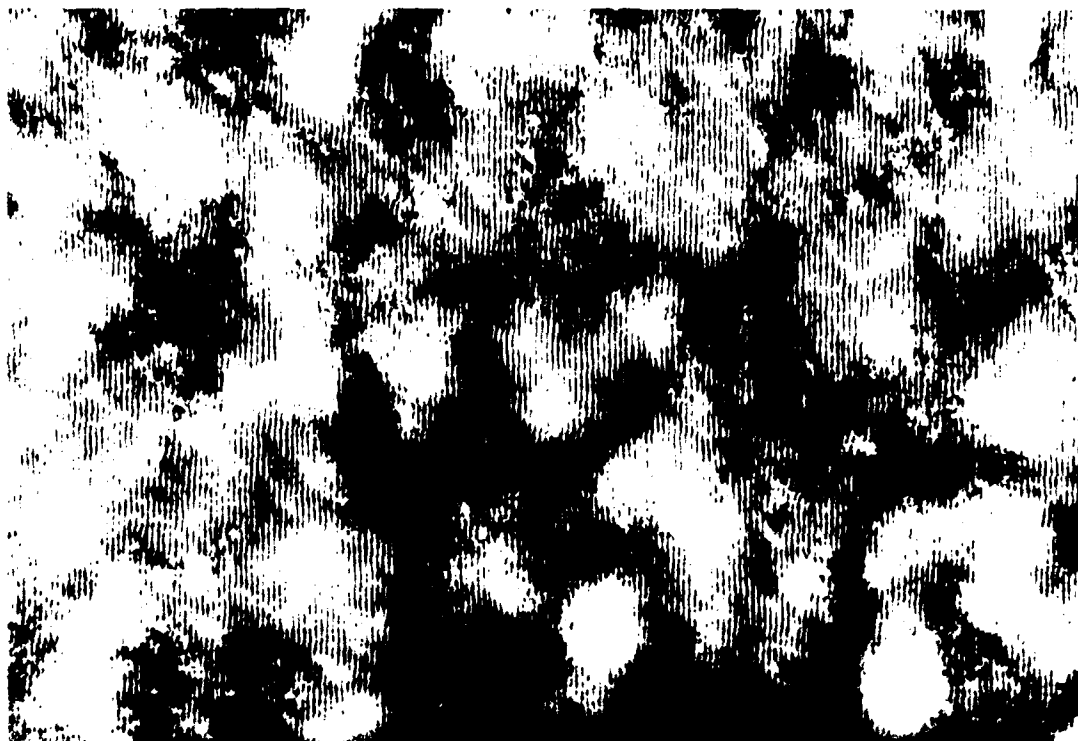
MOIRÉ INTERFERENCE FRINGES AT THE TRANSFORM PLANE OF AN OBJECT
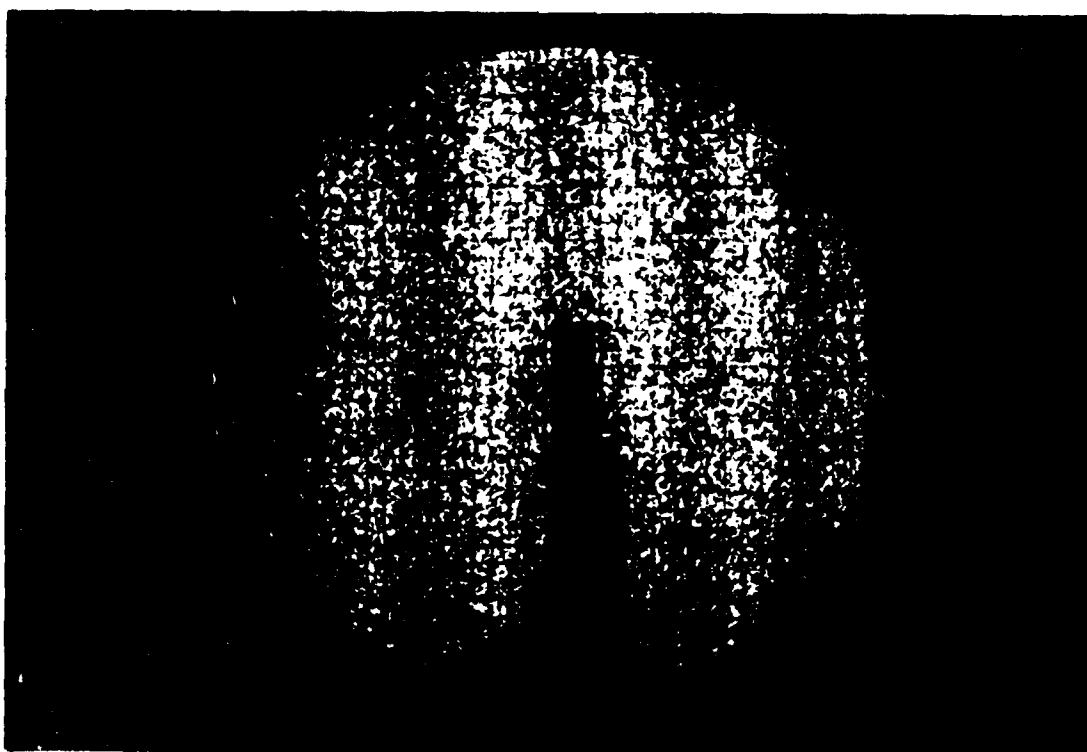
It is quite simple to verify that no other motion of the points A and B in Fig. 1 will yield a moire' pattern that could be confused with that caused by strain. First, translation in the x and y directions (up for x and out of the plane of the drawing for y) will change the phase of both fields by equal amounts and will not change their relative inclination angles in the transform plane, i.e., both field angles will change by the same amount. Translation along the z-axis (to the right or left) will also change the phase of both fields by the same amount and will add curvature to the fields at the transform plane. To first order, this curvature will be equal for both fields and will not change the angle between them. Translations, therefore, will not generate a moire' fringe pattern in the transform plane.

Rotation of the object about the x-axis (through A and B) will obviously not create a moire' fringe pattern, because the points A and B do not move. Rotation about the y axis will change the phase of one field relative to the other, but it will do so uniformly, i.e., the angle between the two fields in the transform plane will not change. Such a rotation will cause the moire' fringe pattern to cycle from maximum to minimum, and, therefore, cause it to scan across the transform plane. Rotation about the z-axis will move points A and B vertically in different directions. This will generate moire' fringes, but they will be parallel to the ω_x-axis and, therefore, be at right angles to those generated by x strain (which are parallel to the ω_y-axis). Shear parallel to the x-axis, like x-axis rotation, will have no effect, since points A and B do not move. Shear parallel to the y-axis will create moire' fringes identical to those of z-axis rotation. The greatest effect that can occur by a combination of strain, translation, rotation, and shear is that the fringes may translate and tilt; however, their spatial frequency in the ω_x direction will always be proportional to x strain.

The system, as shown, has serious drawbacks for strain measurements; strain values corresponding to less than one fringe across the field of view cannot be measured, location of the fringe centers is not accurate, especially as fringe visibility decreases, and no distinction can be made between positive and negative strain. All of these shortcomings can be obviated, as described below, with the introduction of heterodyne interferometry; i.e., creating a phase shift between the two illuminating fields which, in turn, causes the moire' fringes to scan across the output plane.

Heterodyne Interfereometry

One of the most important developments in the last decade in the field of interferometry is the emergence of heterodyne readout of fringe data. For generations, the data presented by interferometers has most often been pictorial. An interferometer divides light beams, directs them through or onto objects under test, and then recombines them to form fringes. Fringes are bands of constructive and destructive interference in a wavefront that presents the

equivalent to a topographical map of optical phase changes between two beams. With the introduction of holography into the field of interferometry, it has been possible to associate fringe patterns with deformations of diffusely reflecting, three-dimensional objects. For qualitative inspection, the pictorial display of fringe patterns is quite useful, but for accurate metrology, it presents a disadvantage. Whereas the conditions that correspond to dark fringes, for example, correspond to exact object displacements, the locations of the centers of the dark fringes may not be precisely defined. Furthermore, the use of dark or bright fringes as data points eliminates many points in the field of view from the measurement process. Because heterodyne methods effectively solve many problems of this sort, they are becoming increasingly important.

Figure 4 illustrates the principle of heterodyne interferometry. The configuration is that of a conventional Mach-Zender Interferometer. A laser beam is partially reflected and partially transmitted by a beam splitter, and the resulting beams are redirected by mirrors to a second beamsplitter that serves to recombine the beams. Before recombination, both beams have been expanded by telescopes, and one has passed through a test object. Changes in optical phase introduced by the test object appear as fringes in the output field. To implement heterodyne readout, a device for constantly changing the phase of one beam is placed in one leg of the interferometer, thereby shifting the optical frequency of this beam. This causes the fringes to scan across the field of view in a constant direction. Electronic circuitry exists that can measure the phase difference between the two signals to within $2\pi \times 10^{-3}$ radians, and in the language of conventional interferometry, this would mean dividing each fringe into 1000 parts.

The advantages of the heterodyne readout are that data may be taken with high precision anywhere in the image fields, with near immunity to variations in light intensity, and in a rapid, machine-readable format. Therefore, an experimental HOSS system, as described in the following section, was designed, fabricated, assembled and evaluated under the present contract.

FIG. 4

HETERODYNE INTERFEROMETER
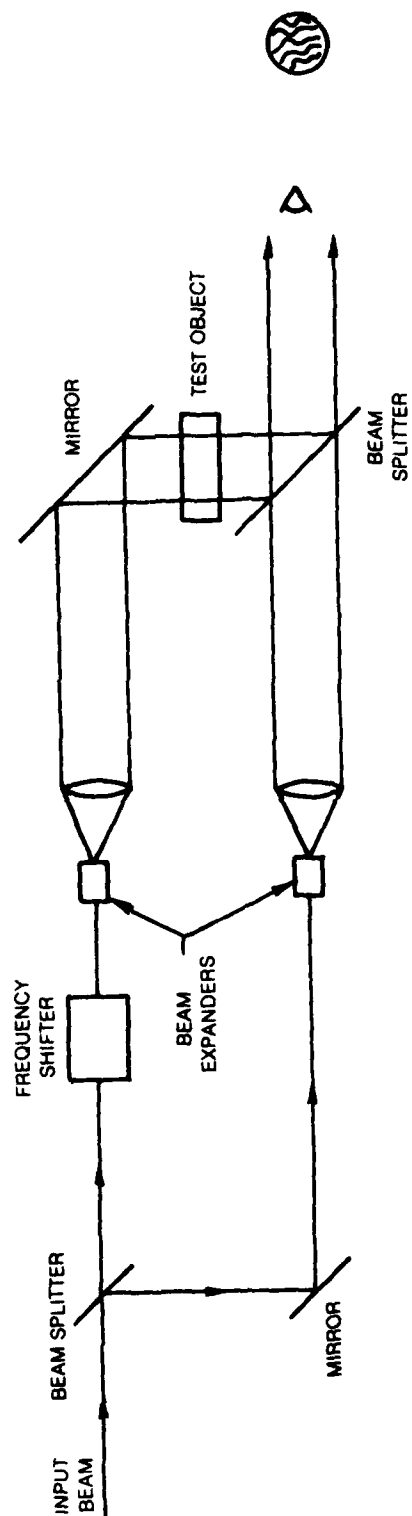
SECTION III

EXPERIMENTAL HOSS SYSTEM

The overall layout of the HOSS system, designed, fabricated and assembled for the experimental investigations described herein, is schematically illustrated in Fig. 5. As shown, the output beam from a HeNe laser is passed through a shutter and reflected by a turning mirror into the heterodyne modulator. The two beams that emerge therefrom are redirected by means of a mirror and beamsplitter to achieve a small angular divergence, passed through a lens, into the strain sensor head, and onto the test object.

The heterodyne modulator, shown in the photograph of Fig. 6, consisted of a rotating half-wave ($\lambda/2$) retarder mounted in a hollow shafted DC torque motor, followed by a quarter-wave ($\lambda/4$) retarder, a Wollaston prism (to separate the frequency shifted beams) and a polarization rotator ($\lambda/2$ plate, to match the polarization of both beams). In operation, when linearly polarized light is incident upon a rotating half-wave retarder plate, the light transmitted will have a linear polarization that rotates at twice the speed of the retarder. This light may alternatively be described as composed of two opposed circular polarizations that are shifted up and down in optical frequency from the original light wave by twice the number of rotation cycles per second. When this light passes through a quarter-wave ($\lambda/4$) retarder whose axis is at 45° to horizontal, the two circular polarizations are converted to vertical and horizontal polarizations, and their up and down frequency shifts are preserved. If the light now enters a Wollaston prism, the two polarizations will be refracted at slightly different angles. After one of the emerging beams is passed through a polarization rotator, the two beams will be polarized in the same direction, and possess a continuous change in phase of four cycles for every rotational cycle of the $\lambda/2$ retarder.

The mirror-beamsplitter is shown in the photograph of Fig. 7, together with the polarization rotator (mentioned in the description of the heterodyne modulator) and the focusing lens.

A detailed schematic of the strain sensor head is presented in Fig. 8, and a photograph of the unit is included as Fig. 9. The two converging beams from the focusing lens are directed to the test object surface by a small mirror, and the light scattered by the object is collected and collimated by two separated lenses, each used on its optical axis, and directed via two mirrors to the recording plane. (The use of two small lenses eliminates the aberrations introduced by a large single lens, as illustrated in the strain sensor concept of Fig. 1.) Recordings are made at the transform plane of the lens on photographic plates that can be precisely relocated. Two detectors are positioned behind the recording plane to receive the light transmitted by the processed plates after relocation. The outputs of the two detectors are fed through two high-Q filters

FIG. 5

OVERALL LAYOUT OF STRAIN SENSOR SYSTEM

11
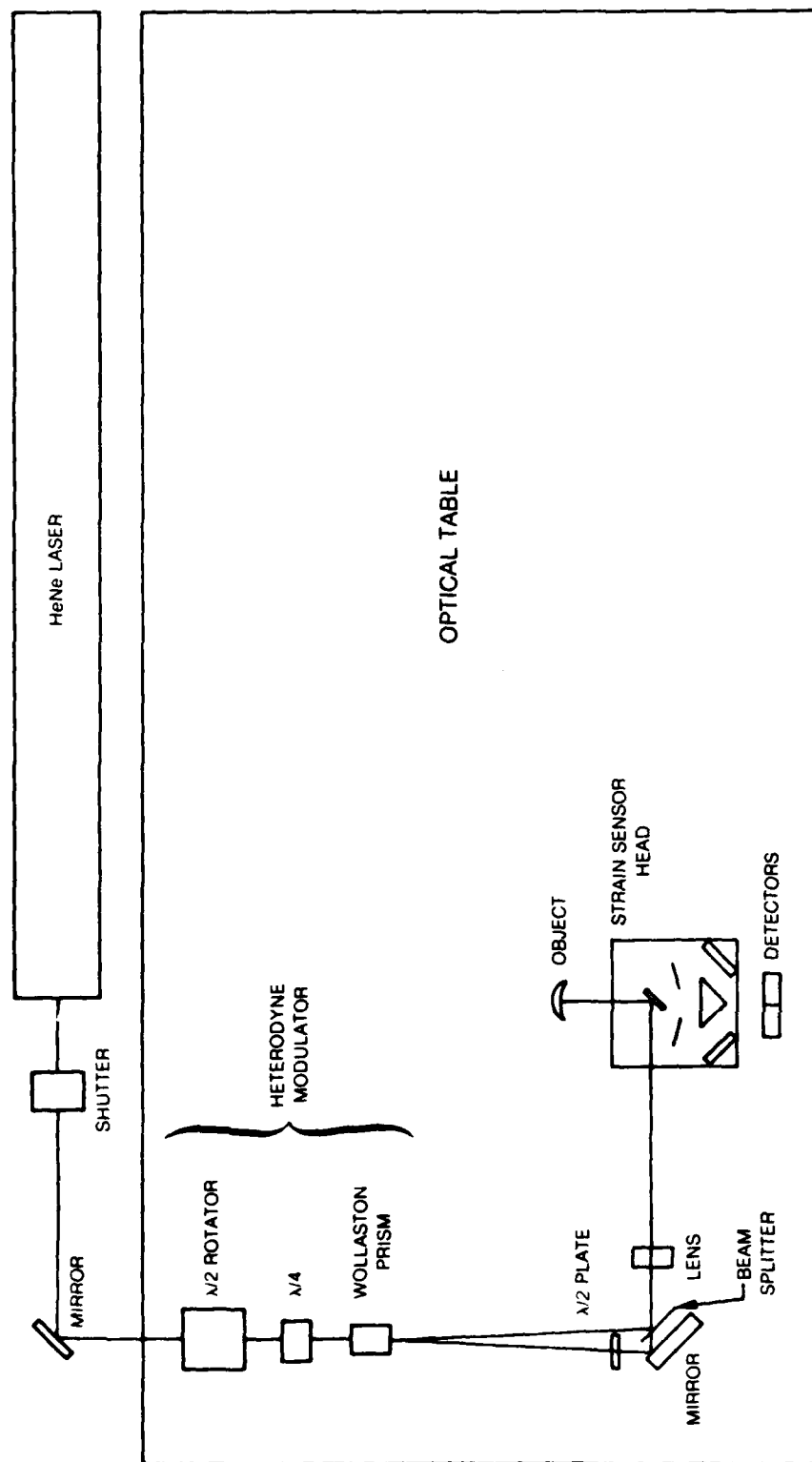
FIG 6

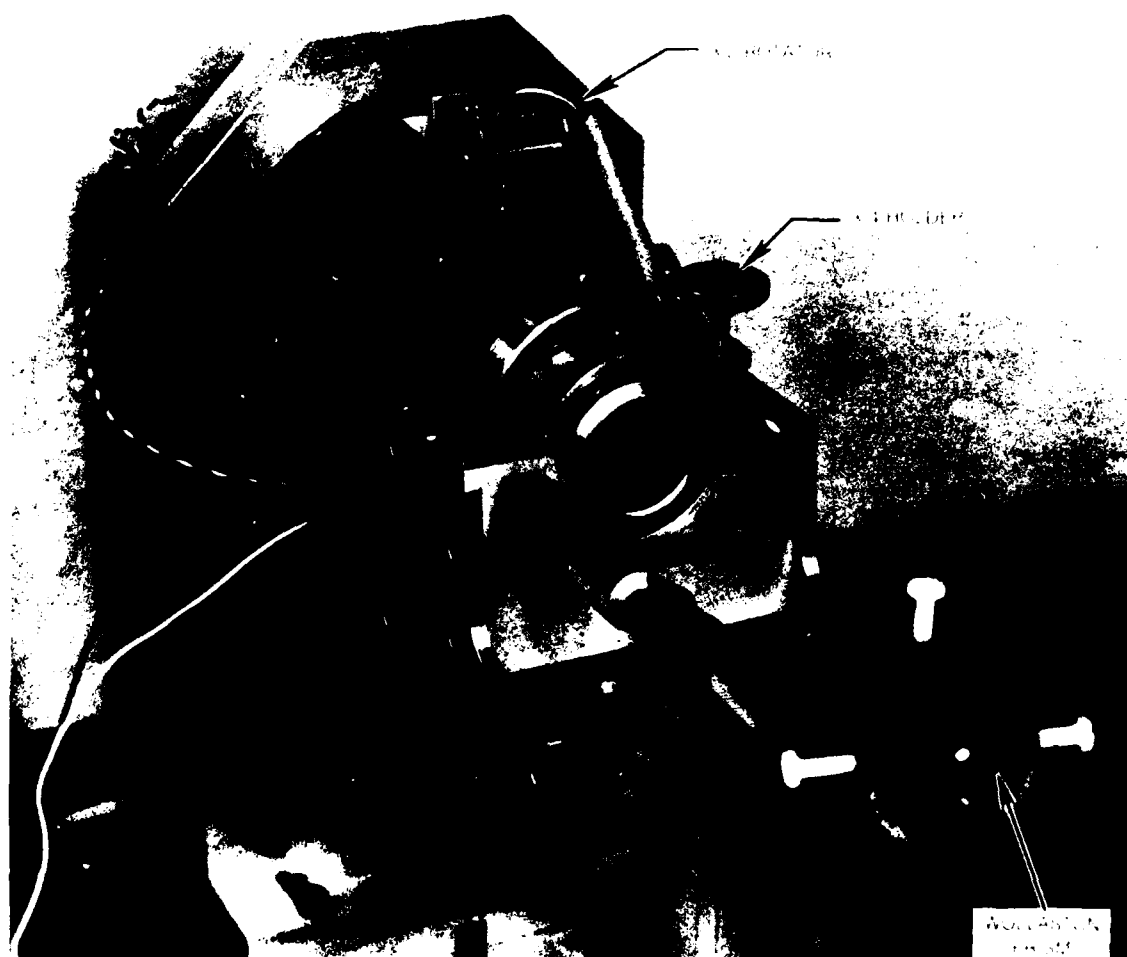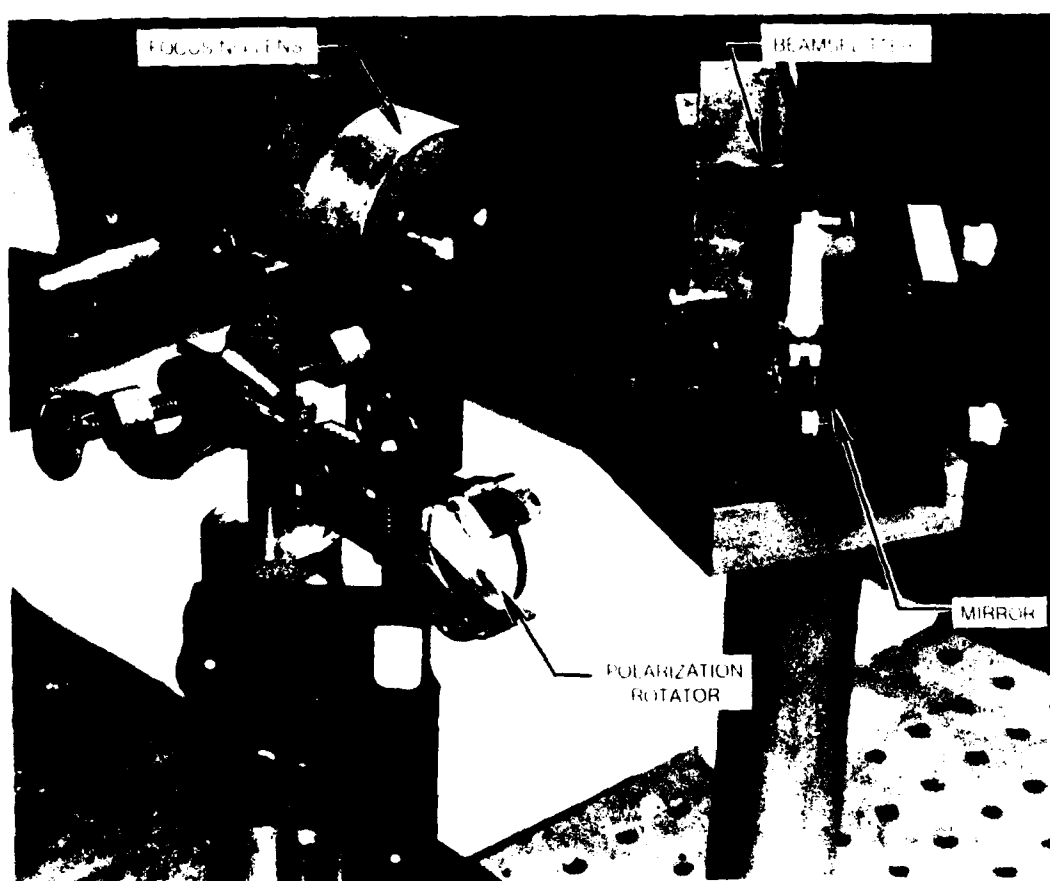**HETERODYNE MODULATOR**

FIG 6

FIG 7

RECOMBINING ASSEMBLY

FIG. 8

PROTOTYPE OPTICAL STRAIN SENSOR SYSTEM

OBJECT

X

Z

d

θ

INPUT BEAMS

MIRROR

LENS

LENS

MIRROR

MIRROR

MIRROR

RECORDING PLANE

14
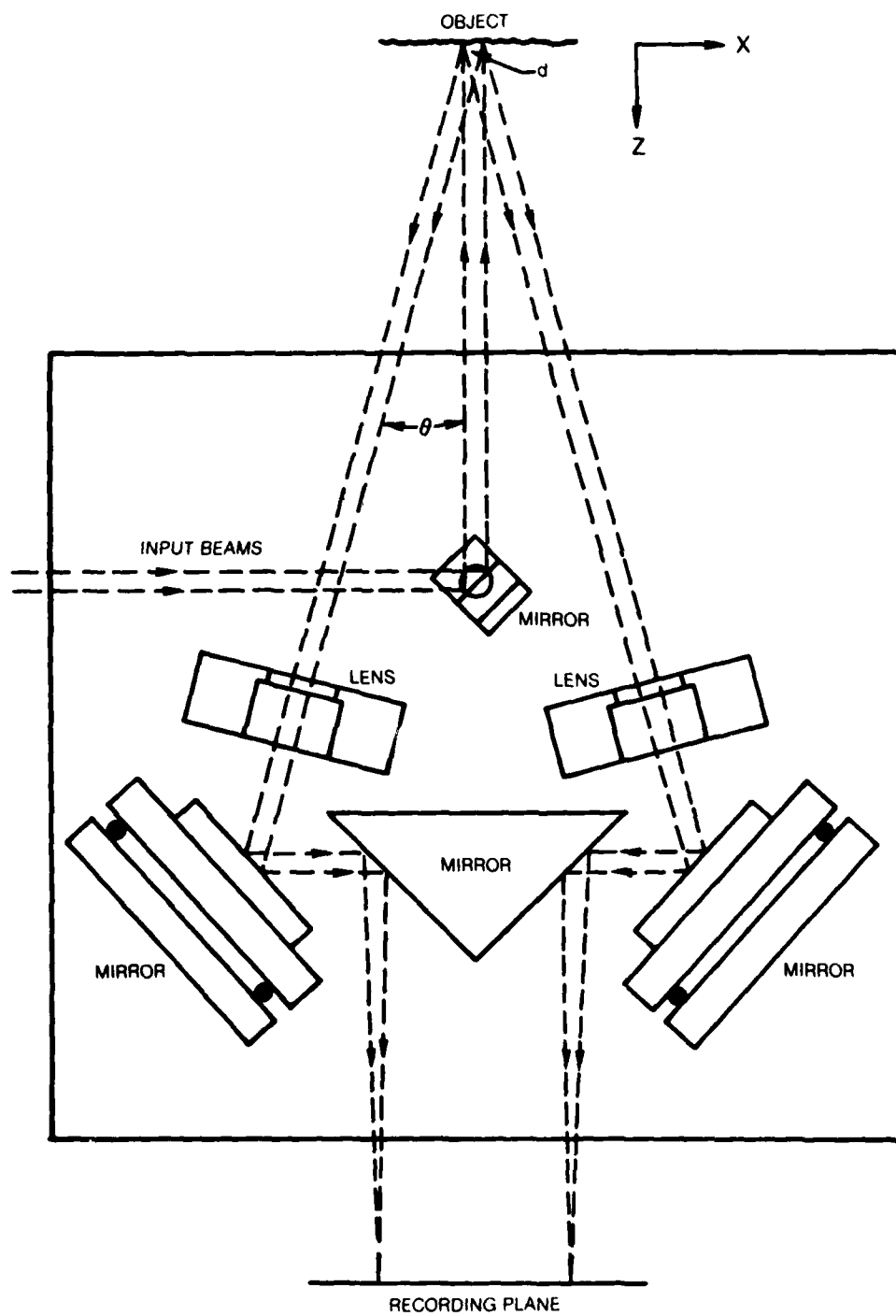
STRAIN SENSOR HEAD

FIG. 9

tuned to the heterodyne frequency and matched for equal phase characteristics. The filter outputs are then fed to a Hewlett-Packard digital phasemeter. Strain is then calculated using the phase difference measurement from the two detectors as discussed in the following major section on STRAIN MEASUREMENT.

Transform Plane Recording Techniques

As part of the investigation, consideration was given to determining the most cost effective method for providing an in-situ recording device for the transform plane recording. It was concluded that, at the present stage of development of the HOSS system, only the straight-forward, in-situ development of photographic plates (as shown in Fig. 9) could be considered reliable enough after study of the following eight potential approaches.

In-Situ Photographic Processing - In this method, a cuvette is constructed that will hold a glass photographic plate immersed in a liquid that can be easily changed. The plate is exposed in water, the water exchanged for a developer, that exchanged for a fixer, and that exchanged for water again. This method has been widely used for in-situ holographic processing, and it has been shown to yield excellent results. The processing time, however, runs into several minutes, largely due to the time needed for the chemicals to diffuse through the emulsion.

Kodak Ektavolt Film - This material consists of an estar film base, coated with a transparent conductor, and then coated with a photoconductor. The photoconductor surface may be charged by a corona discharge, after which, its exposure to light will cause the charge to leak through to the conducting layer. The remaining surface charge pattern may be developed with a liquid toner. The resolution and sensitivity of this material would be more than sufficient for the requirements of the optical strain sensor. However, the need for a corona discharge and the application of a liquid toner are distinct disadvantages. In addition, the material is only available in extremely large quantities (in the order of 7000 square feet) making it impractical for feasibility type experimentation.

Gaseously Developed Film - This material, developed and described by H. M. Smith, et al. of Kodak in Appl. Opt., Vol. 15, No. 3 p. 729 (1976), should provide an excellent system for the needs of the optical strain sensor. However, Eastman Kodak never plans to offer the material on a commercial basis, and will not provide samples of the material, even on an experimental basis.

Thermally Developed Film - Samples of a silver halide film, which develops under heat at about 240°F, were obtained from the 3M Company. This material has excellent resolution and reasonable sensitivity. The disadvantages with the film is that the plastic substrate is not dimensionally stable at the development temperatures, thus, the material would require a rather sophisticated supporting fixture. Furthermore, the film develops best when heated by conduction, rather

than radiantly, because of the rapid increase in its infrared absorption that occurs as it darkens, thereby causing an avalanche effect. Finally, the presence of hot objects in the heterodyne system is likely to affect the accuracy of the measuring system.

ITEK PROM (Pockels Readout Optical Modulator) - This is a device made from a crystal that is both photoconductive and electro-optically active. Exposure to a light field will set up voltage patterns within the crystal that can, by Pockels effect, modulate a readout field. However, the crystal cannot be read out at the same wavelength as the exposing field because the same material is used for both operations. Resolution and sensitivity are not outstanding, but would be adequate if it were otherwise acceptable.

Thermoplastic Film - Devices are commercially available for rapid holographic recording using thermoplastic film. However, this material gives a phase image that is not suited to the optical strain sensor. In addition, thermoplastics have a spatial bandpass characteristic that give them practically no response at the low spatial frequencies used in the optical strain sensor.

Hughes Liquid Crystal Light Valve (LCLV) - This device combines a photoconductive layer with a liquid crystal layer. The first provides a spatially varying charge pattern when exposed to light, while the second converts this to a modulation pattern in a readout field; the two fields can be completely isolated. Units currently available are made for TV projectors, or for optical data processing, and thus are not able to function as storage devices but rather, operate only in real-time. Storage devices have been made by Hughes in the past, but considerable incentive would have to be provided to induce them to make a special run of such devices. Two LCLV units were obtained from Hughes on loan and were evaluated. The sensitivity was found to be quite low (marginal for the optical strain sensor application), while the resolution was judged to be adequate.

Wafer Image Intensifier - A novel approach to the problem of in-situ recording was conceived that would utilize a wafer image intensifier. Such devices consist of a photoemissive surface, a microchannel plate, and a photophosphor. The microchannel plate (MCP) is a structure consisting of many parallel microscopic tubes, the inside surfaces of which are prepared for secondary electron emission. When placed in a vacuum with a voltage across the surfaces, electrons entering the tubes cause an avalanche of electrons due to collisions with the walls. These are accelerated through the tubes, each of which acts therefore like a miniature photomultiplier. Because of the high electron gain of the MCP, a faint image on the photoemissive surface is converted into a bright image on the phosphor.

If such a device were built with the possibility of optical feedback between the phosphor and the photoemitter, it should exhibit a threshold of input light level above which it would become regenerative. In this mode, the

17

output phosphor would provide sustaining illumination to the photoemitter, and that region of the intensifier would saturate. The device would thus be optically bistable. An optical pattern exposed onto the device could saturate, and thereby deactivate all regions of the device where the light was above threshold. The remaining areas could then be used as photodetectors with the input light field at a reduced level. This device could thus combine both the photodetector and the recording system. Development of such a device should be considered for future possibilities in systems like the optical strain sensor.

In-Situ Photographic Processing

Based upon the above considerations, a liquid gate for the in-situ processing of photographic plates was fabricated, installed and evaluated. Testing of the system indicated that processing times as short as five minutes are quite easily obtained. This is based upon a minimum time requirement of four minutes for total development and fixing. The additional minute is required for loading the plate, and for changing the chemicals. Although data can be read out while the gate contains the fixing solution, it is preferable to replace the fixer with water if the plate is to be used for a matter of hours.

The exposure times required for the proper density of development are shorter, by a factor of two or three, than those required with dry plates. This is quite consistent with published data on in-situ holographic processing, and it is due to the sensitizing effect of water. The signal levels obtained with the in-situ plates are comparable to those obtained with dry plates.

The stability of the in-situ processed plates was tested by performing a long term drift test. A recording of an unstressed sample was made and left unstressed while the phase of the heterodyne detectors was monitored. A plot of the apparent strain during six hours of elapsed time is presented in Fig. 10. (The dashed portions of the curve indicate intervals during which data was not taken.) While there is no ready explanation for the slight negative strain observed initially, it can be noted that the peak of the curve occurred during the early afternoon, possibly suggesting that the drift may be correlated with laboratory temperature.

HOSS System Parameters

Parameters of importance in calibrating the sensor head are the separation between the two illumination beams (or spot separation), and the angles subtended by the illumination directions and the two observation directions. The separation between the illumination beams is measured by a knife edge on a translation stage. The two beams are directed to the knife edge by a mirror, and a detector is used to indicate the amount of flare from the edge. The positions corresponding to the maximum flare from each spot are noted from the micrometer on the stage and the spot separation is computed. It was shown that a photodetector could be used to locate this to within 0.0005 inches.

18

FIG. 10

TEST OF LONG TERM STABILITY

MICROSTRAIN (APPARENT)

HOURS
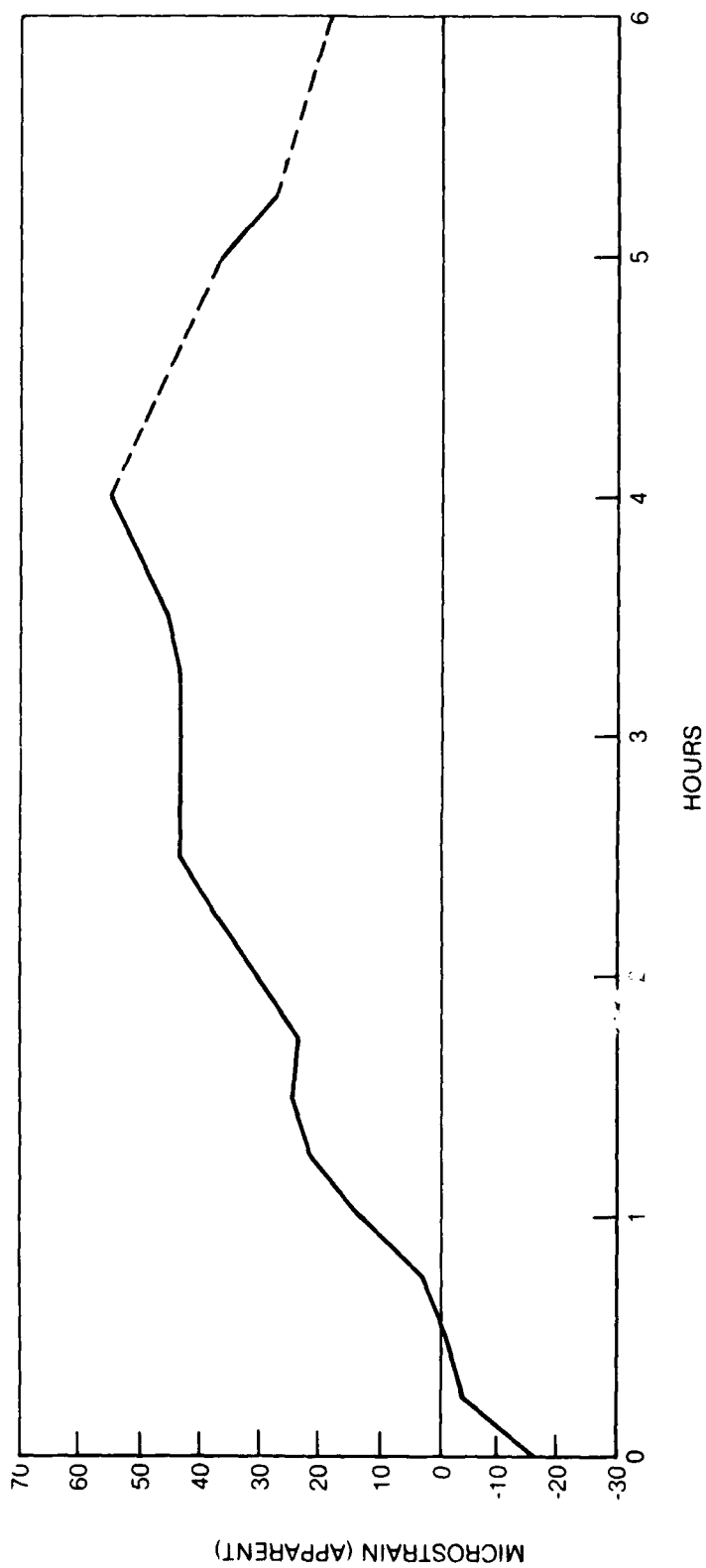
The angles between the illumination directions and the two observation directions are determined by mounting a small rotational stage on a post which is notched halfway through so that the two beams will illuminate a surface at the center of rotation of the stage. A knife edge is fastened to the moveable portion of the stage, on an arm, so that it can pass in front of the two lenses as the stage rotates. A polarizer is placed between the rotating half wave plate and the quarter wave plate, which has the effect of modulating both beams. This signal is measured by the gain portion of the Hewlett-Packard gain-phase meter while the blade is passed in front of one of the lenses. The angle at which the signal on that channel is one-half its original value, is recorded. Similarly, the angle at which the signal from the other channel is reduced by one-half, is recorded. The difference between these two angles is the included angle between the two detectors, and this can be measured to 0.1°.

Employing the strain calculation equation (as discussed in the following section on STRAIN MEASUREMENT):

$$\varepsilon = (\phi/360)(\lambda/2d \sin\theta),$$

a series of curves can be drawn up to indicate the loci of constant sensitivity. Presented in Fig. 11 is a plot of spot separation d versus θ, the half-angle subtended by the detectors, for constant values of the strain required for one cycle of phase change between the two heterodyne signals. (φ in the above equation represents the phase difference in degrees.) These curves are useful in determining the strain accuracy as a function of these two geometric parameters in the experimental setup. If phase can be measured to 10^{-3} cycles, for example, the 1000 microstrain/cycle curve corresponds to the operating points along which the strain sensitivity would be 1 microstrain.

Another parameter of importance is the distance from the recording plane to the lenses; this distance should be equal to the focal length of the lenses (124 mm for the prototype system). The precise setting of this distance is essential to the suppression of false strain indications caused by out-of-plane translations. With convenient system parameters (spot separation of 1.0 mm and angles of ± 14.4°) an error of 6 mm in this distance (124 mm) will cause an error of 7.2 microstrain for each 25 micrometers of out-of-plane displacement. The procedure for setting this distance is to actually measure the sensitivity of the setup to out-of-plane displacement by physical translation of the object. The object to lens distance is not a critical parameter, but must be known to determine the observation angles.

FIG. 11

LOCI OF CONSTANT SENSITIVITY

SPOT SEPARATION-mm

HALF-ANGLE-deg

MICROSTRAIN/CYCLE

120
150
200
300
500
1000
2000

21
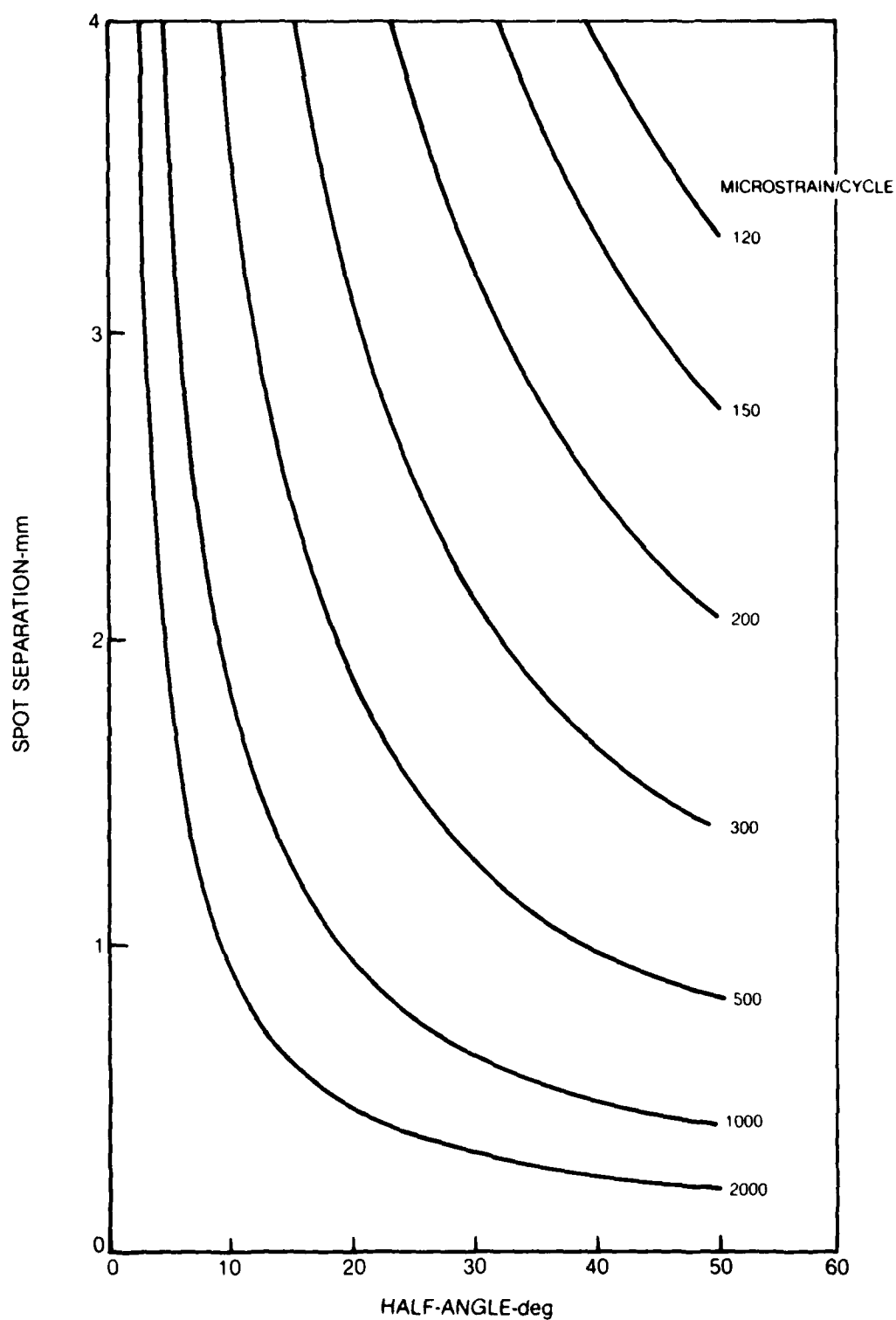
A final parameter of interest is the effect of increasing strain on the detector output signal strength. A typical measurement graphically depicting this relationship, is presented in Fig. 12. This is the result of flexing the object surface (a beam under 4-point bending) which causes the spectrum of one spot to translate in a direction opposite to that of the other spot. The loss of signal strength has an indirect effect on the strain measurement in that the phase measurement is influenced somewhat by background noise coming from the detectors that may originate from ambient lighting, air currents, vibration, and subfrequency modulation by the rotating $\lambda/2$ retarder plate.

SIGNAL STRENGTH VS. STRAIN

23
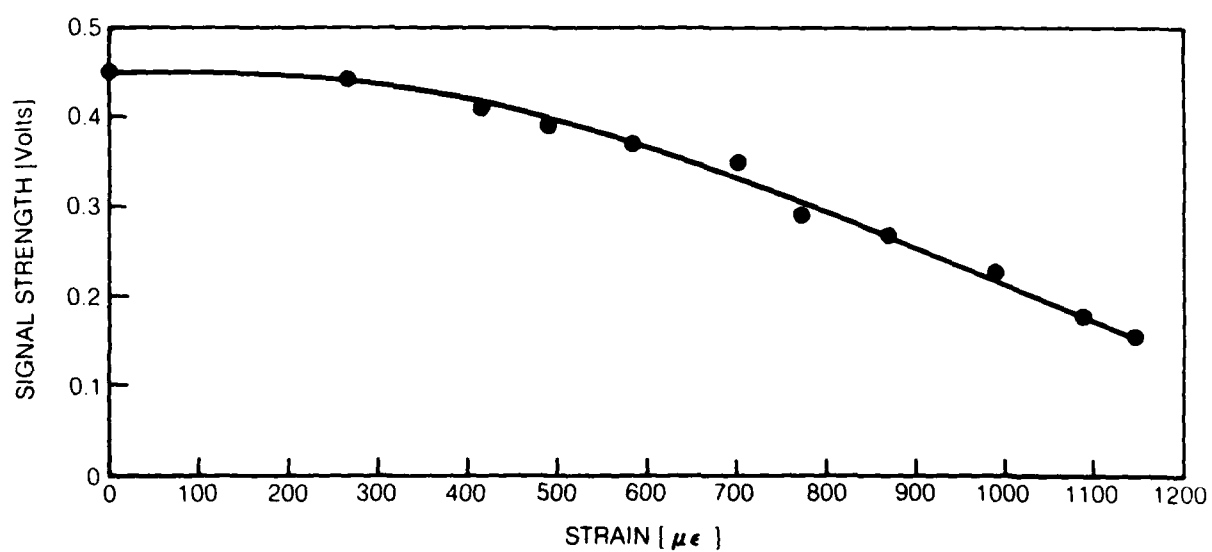
SECTION IV

STRAIN MEASUREMENT CALCULATION PROCEDURES

Static Strain

When the HOSS system described and discussed in the previous section is used, static strain on an object surface will be directly proportional to the difference in phase of the heterodyne signals from the two detectors. This phase difference is obtained by direct evaluation of the two signals by an electronic phasemeter (a Hewlett-Packard digital unit for these studies). These commercially available instruments usually operate by amplifying the two input signals and hard limiting them to convert them to square waves. The elapsed time is measured between the leading edge of one square wave and the leading edge of the other, and is then divided by the time period of one cycle. This may be averaged over a number of cycles to improve accuracy. Strain is then calculated by multiplying the phase difference ϕ (in degrees) by an appropriate scale factor based on the geometric parameters of the system (see Fig. 8):

$$\epsilon = (\phi/360)(\lambda/2d \sin\theta),$$

where the geometric parameters are:

λ - the wavelength of the illumination beam.

d - the separation of the two illuminated spots on the object surface

θ - the angle between the surface normal and the directions in which the transform fields are sampled, or the half-angle of the beams sampled by the detectors.

An appropriate spot separation, or equivalent gage length, was taken to be 1 mm; a convenient half-angle for the system was in the order of 15 degrees; and the wavelength used in these investigations was 0.6328 microns (HeNe laser).

Vibratory Strain

When an object vibrates in the HOSS system, the output of either detector takes on the form of a sine function consisting of the sum of a linear function of time and a sinusoidal function of time. In this type of output, the amplitude of the sinusoidal time function (which corresponds to a phase vibration amplitude) is not directly obtainable by a phase measurement. However, the phase vibration amplitude can be obtained by counting the number of zero crossings of this signal

24

over a large number of heterodyne cycles, and dividing by the number of vibration cycles. For this method it is desirable to have the heterodyne frequency irrational to, and well below, the vibration freuency. Furthermore, the calculation of strain requires measurement of the difference between the phase vibration amplitudes of the two channels.

These requirements have been effectively met through the use of a reversible counter which can make a positive count for each positive going zero crossing of one signal and a negative count for each positive going zero crossing of another signal. This counter was gated from the gate output of a second counter that was equipped to measure frequency ratios. When the two detector outputs were connected to the reversible counter, and the vibration signal connected to the "divide-by" input of the second counter, the reversible counter would display the difference in the number of positive going zero crossings of the two detector signals that occurred during 1,000 10,000 etc. cycles of the vibration signal. (The number of vibration cycles could be chosen by a selector switch.) It was also possible to connect the heterodyne signal to the "divide-by" input and the vibration signal to the "divide-into" input, and thus count over 1000 heterodyne cycles. In this case, the two counter displays had to be divided to obtain the desired answer.

The logic of this vibration detection scheme was given thorough consideration, and can best be discussed with reference to Fig. 13 where two curves have been drawn; the upper curve representing the vibration signal impressed upon the object, and the lower representing the output of the detector. The object vibration causes the fringes to sweep back and forth across the detector, while the heterodyne signal causes them to translate with a constant velocity. The vertical lines mark the periods of the vibration cycle. The electronics detect and count the positive going zero crossings in the detector output signal for a time interval equal to 1000 or 10,000 vibration cycles. The resulting number, when normalized, gives the number of positive going zero crossings per vibration cycle and, for a large number of vibration cycles, this converges to the peak to peak vibration amplitude in fractions of π phase shift. In Fig. 13, for example, 23 positive going zero crossings can be counted within 10 vibration cycles yielding a vibration amplitude of 2.3. (The exact value was 2.4.)

A question arises, however, as to how the method works when the vibration amplitude is small, as shown in Fig. 14. Clearly, if the amplitude were zero, the electronics would count the number of zero crossings generated by the heterodyne signal alone. This would persist until the vibration amplitude exceeded the ratio of the heterodyne frequency to the vibration frequency. This, then, is the value beyond which the vibration signal would cause local maxima and minima, and thus would begin to influence the number of zero crossings. The question posed is this: does the heterodyne signal generate an excess number of zero crossings that should be subtracted from the total count to obtain the correct vibration amplitude? The answer to this question could only be obtained by modeling the process on a computer, and the results are presented in Fig. 15.

25

FIG. 13

EXAMPLE OF THE VIBRATION DETECTION SCHEME

UPPER CURVE — VIBRATION SIGNAL
LOWER CURVE — DETECTOR OUTPUT
● — POSITIVE GOING ZERO CROSSINGS
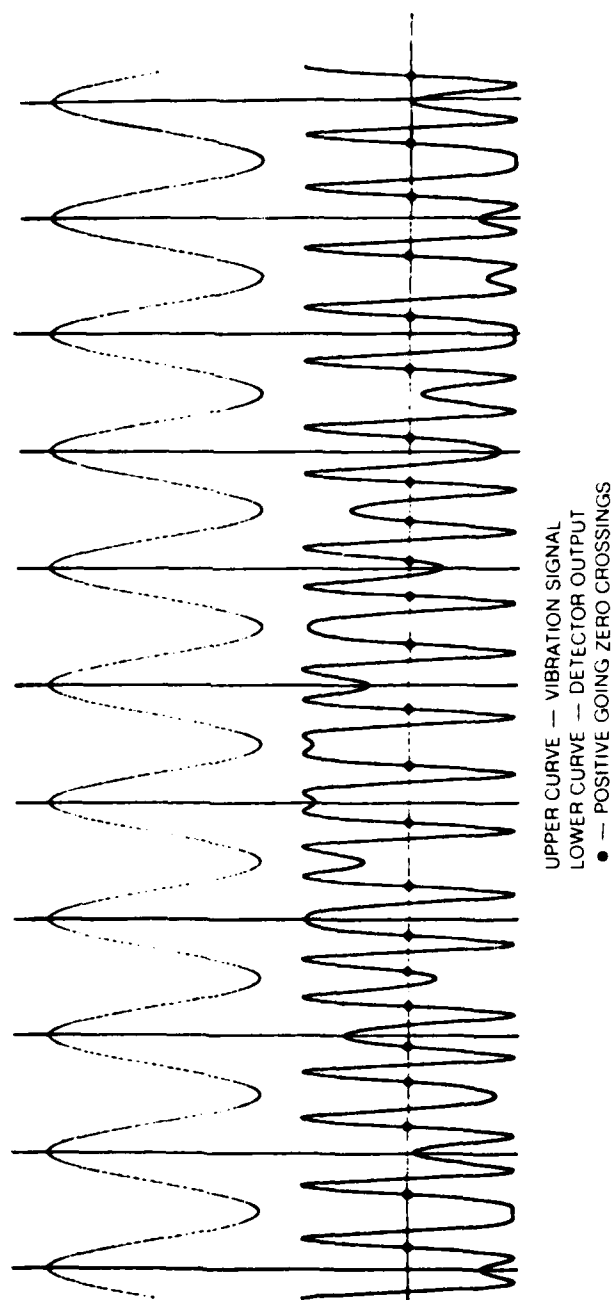
DETECTOR OUTPUT FOR A REDUCED LEVEL OF VIBRATION

● — POSITIVE GOING ZERO CROSSINGS

FIG. 14

27

FIG. 15
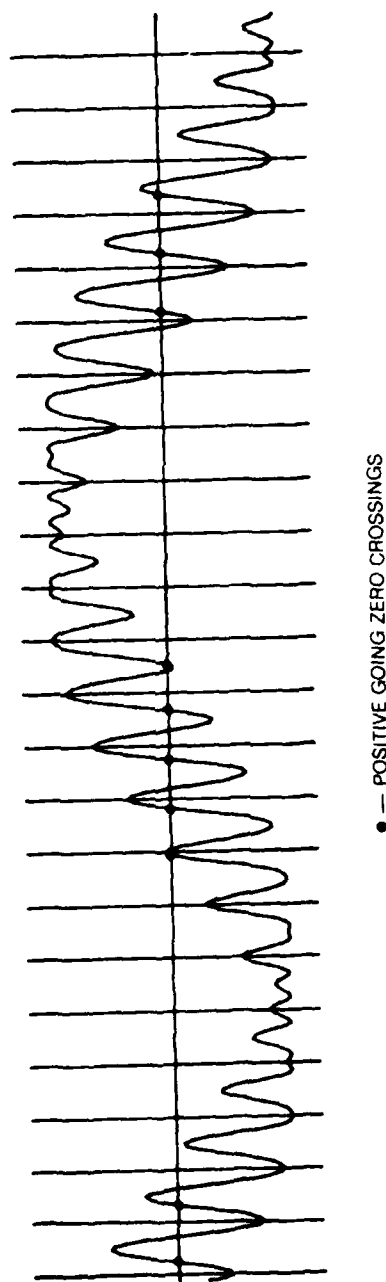
ZERO CROSSINGS vs VIBRATION AMPLITUDE
(COMPUTER MODEL)

PEAK TO PEAK VIBRATION AMPLITUDE
(FRACTION OF π RADIANS)
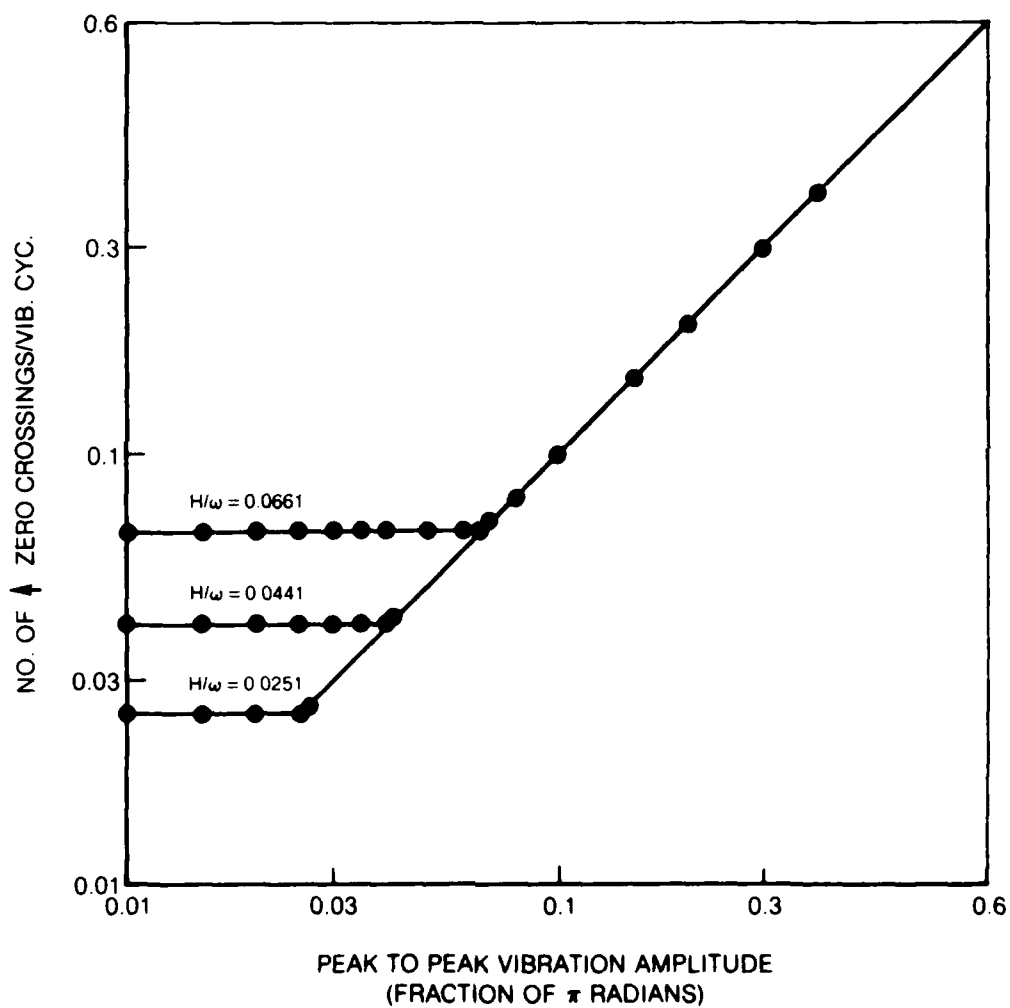
Computations were made of the number of upward (positive going) zero cross-ings of $\sin(Hx+A\sin\omega x)$ in 10,000 cycles of $\sin\omega x$, for various values of the vibration amplitude, A, and for three ratios of H/ω. The normalized results of these computations are plotted in Fig. 15 as a function of the vibration amplitude. The plots demonstrate that the system makes a sharp transition from counting the zero crossings due to the heterodyne signal, to a count that yields almost exactly the vibration amplitude. Clearly, the heterodyne signal does not generate an excess number of zero crossings and therefore no subtraction is required.

SECTION V

ANALYTICAL INVESTIGATIONS

Several areas of interest were examined theoretically throughout, and prior
to, the conduct of these investigations. Considered below are the topics of
sensitivity and accuracy, measurement range, object translations, surface tilt
and general limitations; along with discussion of experimental work related to
translations and tilts.

Sensitivity and Accuracy

The sensitivity of the optical heterodyne strain sensor due to the detectable
signals will equal or exceed most strain gages. This comes from the ability of
electronic signal comparators to measure phase to one part in 10^3. Based on
this, the sensitivity would be

$$\Delta\varepsilon = \lambda\Delta\psi/d2\sin\theta,$$

where $\Delta\varepsilon$ is the sensitivity of the strain measurement, λ is the wavelength of
light, $\Delta\psi$ is the sensitivity of the phase measurement in fractions of a cycle, d
is the gage length (distance between the spots), and θ is the angle of the detec-
tors to the normal. With $\lambda = 0.633$ nm, $\theta = 30°$, and $\Delta\psi = 10^{-3}$, we have $\Delta\varepsilon = 0.633$
microstrain/mm gage length. Clearly, the accuracy of the system would depend
upon the precision with which θ and d could be measured, and one percent accuracy
in these parameters should be easily achieved.

Measurement Range

The range of measurement is determined by the illuminated spot sizes, and two
factors compete in this choice. For the range of strain measurement, the displace-
ment of the object surface under one illuminated spot should not exceed 1/5 of the
spot diameter. Thus, the range may be estimated as

$$\varepsilon_{max} = S/5d,$$

where ε_{max} is the maximum strain, S is the spot diameter, and d is the gage
length. If the illuminated spots are 0.1 mm in diameter, $\varepsilon_{max} = 20,000$ micro-
strain/mm gage length. Rotations, however, will shift the speckle patterns that
fall on the detectors, and these must not move by more than 1/5 of a characteri-
istic speckle diameter. Thus, the maximum rotation allowed would be on the order
of

$$q_{max} = \lambda/5S,$$

where σ is the rotation of the object surface. With illuminated spots of 0.1 mm, $q_{max} = 1,200$ microradians, independent of gage length. In designing a practical system, some range in strain measurement would probably be sacrificed to obtain less sensitivity to rotations by the choice of a smaller illumination spot.

Object Translations

When the distance between the transform lens and the recording plane is exactly equal to the focal length of the lens, only parallel rays from the object will intersect at any given point in the transform plane (see Fig. 8). When this condition is not met, the corresponding rays coming from the object appear to diverge from a common point as they leave the object (or conversely, they appear to converge if the defocusing is in the opposite direction). Translations of the object, under this condition, can give phase changes through one channel of the strain sensor that differ from those through the other channel, and the difference will appear as false strain. A similar effect will be present when the two illumination beams are not parallel; however, the phase change resulting from this effect will be equal in both channels and will be eliminated by the phase difference detector.

The defocusing problem encountered here is strictly analogous to that of fringes generated in hologram interferometry by object translations in the presence of curved perspective, (Ref. 4). This greatly simplifies what might otherwise be quite a complex analysis of all the vectorial relationships involved. Let us assume that the object translates along a vectorial displacement, L. If a double-exposure hologram were recorded, one exposure before and one after the translation, fringes would appear across the surface of the object due to linear variations in the phase change created by the translation. The linear variations in phase change may be described by a fringe vector, K_f, whose scalar product with a space vector, d, connecting the two illuminated points on the object surface, yields the differential phase change between the two points. This differential phase change is exactly the change in phase that occurs in the output signal of one detector of the strain sensor relative to a reference signal. If subscripts a and b are used to denote the two channels of the strain sensor, we may write the following equations for the two phase changes ϕ_a and ϕ_b:

$$\phi_a = d \cdot K_{fa} \text{ , and } \phi_b = d \cdot K_{fb} \text{ .}$$

When only a translation and a curved perspective generate fringes in hologram interferometry, the fringe vector has the simple form

$$K_f = L_{ob} \, 2\pi/\lambda R_{ob} \text{ ,}$$

where R_{ob} is the radius of the observer's perspective, and L_{ob} is the portion of L that is normal to the observing direction. L_{ob} may be referred to as the normal projection of L onto a plane perpendicular to the viewing direction, and it is related to the total translation by a projection matrix, P_k (Ref. 5). Thus

$$L_{ob} = P_k L \quad .$$

The phase difference between the two channels of the strain sensor may now be written as

$$\Delta\phi = (2\pi/\lambda) \ d \ (P_{ka}/R_a - P_{kb}/R_b) \ L,$$

where R_a and R_b are the distances from the object surface to the points where the rays converge, or from which they diverge, due to misfocusing. The projection matrices may be written in terms of the unit vectors of observation, k_a and k_b as

$$P_{ka} = I - k_a \otimes k_a, \quad \text{and} \quad P_{kb} = I - k_b \otimes k_b$$

The operator $k \otimes k$ generates the matrix

$$k \otimes k = \begin{bmatrix} k_x^2 & k_x k_y & k_x k_z \\ k_y k_x & k_y^2 & k_y k_z \\ k_z k_x & k_z k_y & k_z^2 \end{bmatrix} ,$$

where $k = \hat{i}k_x + \hat{j}k_y + \hat{k}k_z$.

The following simplifying assumptions can be made. The vector "d" may be considered to lie in the x direction, and the observation directions may lie at $\pm \ \theta$ to the surface normal of the object and in the x, z plane. With these assumptions the phase difference becomes

$$\Delta\phi = (2\pi/\lambda) \ d \ [L_x \cos^2\theta(1/R_a - 1/R_b) - L_z \sin\theta \cos\theta \ (1/R_a + 1/R_b)]$$

where L_x and L_z are the x and z components of the object displacement. Proper adjustment of the system will make both R_a and R_b approach infinity simultaneously, and under this condition the system output will be immune to object translations.

In the experiments that were performed, the object was placed upon an x, z translation stage and the transform plane recording on a z translation stage. A recording was made and the z position of that recording adjusted until no phase change was observed for a z translation of the object. The sensitivity of the system to x translation was then checked and found not to be zero. It was concluded, after the above analysis, that the z position of the recording had been adjusted until the defocusing was equal and opposite for the two channels, (i.e., $R_a = -R_b$). Examination of the phase change of each channel relative to the phase of the rotating $\lambda/2$ waveplate confirmed that these phase changes, as functions of object z position, were zero for different settings of the recording plane. It was found for this

32

breadboard setup that a small adjustment in the lens position corrected the problem, and proper alignment was obtained. The conclusion is that some small axial adjustment of one of the lenses would be desirable for an instrument of this type. When the system was properly adjusted, z axis translations of the object in the order of several tenths of an inch could be tolerated. Translations in the x direction, however, gave a severe drop in output signal if more than ± 50 microns were introduced. This corresponds to a significant fraction of the approximately 100 micron spot size.

Surface Tilt

In the experimental measurement of vibratory strain, tilt of the object surface appeared to limit the amount of strain that could be evaluated. This surface tilt could affect the measurement of strain in two ways and it was not certain which imposed the real limit. First, the surface tilt introduces a common phase modulation into both detector channels that is eliminated by subtracting the pair of measurements. In the case of vibratory strain, this additional modulation increases the frequency bandwidth of the detector signals. If the bandwidth of the detector electronics is exceeded, the signal strength will drop and the readout system, based upon sensing zero crossings, will not perform properly. Alternatively, however, the surface tilt also translates the illumination pattern in the transform plane of the optical strain sensor relative to the recording that was made there. Because of the random nature of the field at the transform plane and the recording, translation between the two leads to decorrelation and loss of moiré interference. This also reduces signal strength and thus causes the readout system not to perform properly.

Laboratory experiments demonstrated that it is the second of the two mechanisms mentioned above that limits the maximum amount of strain that the optical strain sensor can measure, and that the sensor performance for vibratory strains cannot be extended greatly by increasing the bandwidth of the detector electronics. Figure 16 shows plots of detector signal strength versus phase shift for two types of static displacements, pure surface tilt and tilt that accompanied bending. Both curves show substantial loss of signal after a phase shift of ± 2 or 3 cycles. Both curves also show curious asymmetries, which were reproducible, and for which no explanation can be provided. The reduction of signal strength is less of a problem for the measurement of static strain than for vibratory strain. With static strain, the signals are filtered through high Q filters to remove the effects of noise and harmonically related frequencies, and the readout is provided by a phase meter that is quite insensitive to signal amplitude. For vibration measurements, this type of filtering cannot be performed and the readout system is more sensitive to the quality of the signals.

It is possible to derive a relationship between the maximum surface tilt that can be tolerated and the maximum strain that can be measured for a plate that is bent to a cylindric . arc, as shown in Fig. 17. Let R be the radius of curvature of the neutral surface of the plate, and let ΔR be the distance from the neutral surface to the outer surface. Strain, ϵ, may be defined as

FIG. 16

SIGNAL STRENGTH vs PHASE SHIFT

PURE TILT

BENDING

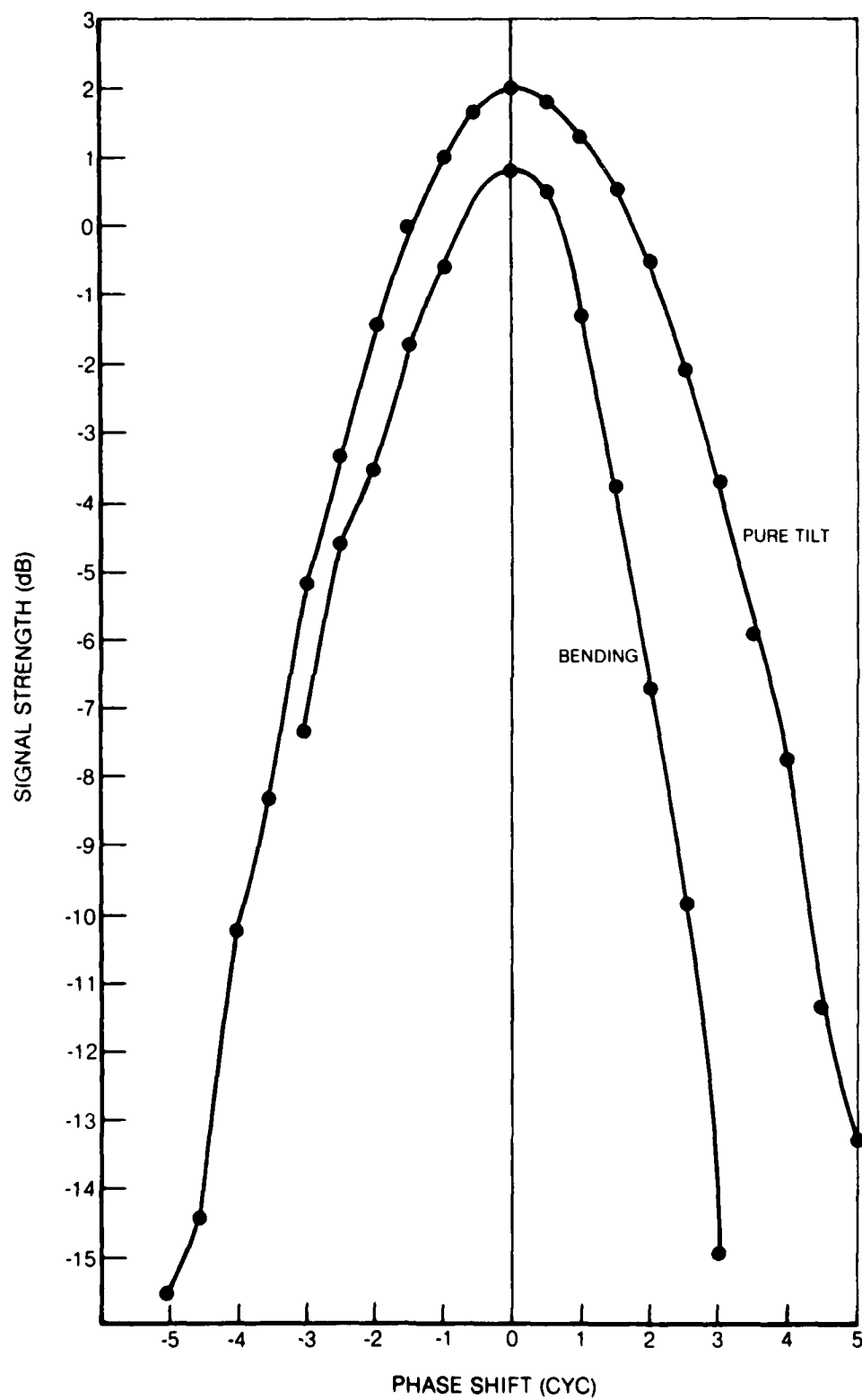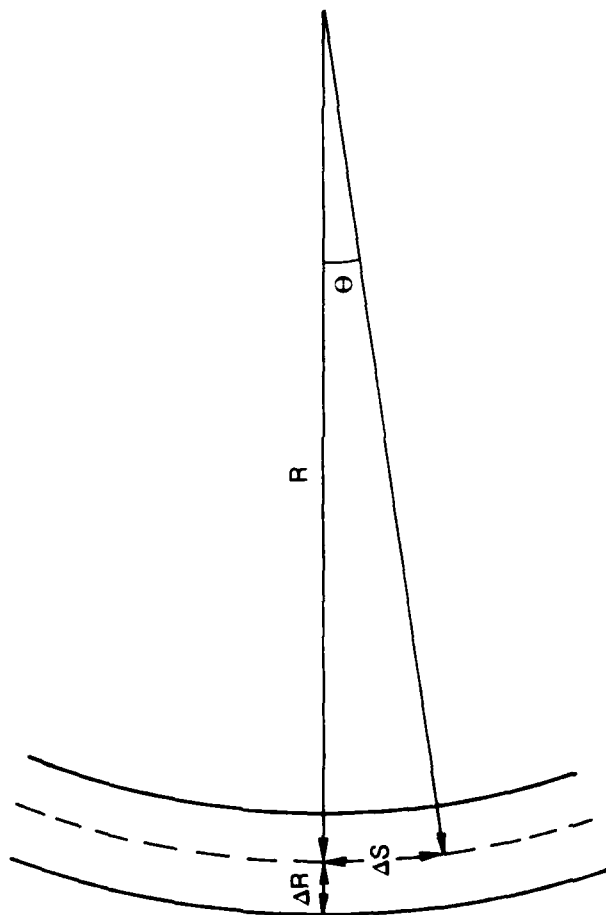SIGNAL STRENGTH (dB)

PHASE SHIFT (CYC)

FIG. 17

BENDING AND SURFACE TILT

$$\varepsilon = \Delta R/R.$$

The surface tilt, i.e., the angle θ through which the surface has been rotated, may be defined as the ratio of the arc length, ΔS, to the point of no rotation, divided by the radius of curvature, i.e.,

$$\theta = \Delta S/R.$$

Combining these equations, and considering the maximum values for θ and ε, gives

$$\varepsilon_{max} = (\Delta R/\Delta S)\, \theta_{max} \quad .$$

If N is the number of plate thicknesses from the point of no rotation to the point where strain is measured, then the maximum strain that can be measured is related to the maximum allowable rotation by

$$\varepsilon_{max} = \theta_{max}/2N$$

Clearly, the thinner the plate, relative to its lateral dimensions, the more severe this problem becomes. The maximum allowable rotation is inversely proportional to the diameter of the illuminated spots on the object surface. Greater tolerance to surface tilt may be obtained, therefore, only at the expense of less tolerance to lateral displacements of the object.

General Limitations

In addition to the measurement limits due to surface tilt, another restriction on the HOSS is that the spots illuminated have to remain under the illuminating beams during the entire cycle of measurement. This limitation is in a way analogous to the requirement for proper bonding of a resistive strain gage. In addition, the surface under measurement has to retain its integrity of microstructure during the measurement: i.e., little, if any, erosion or build-up of dirt can be tolerated. Finally, any phase changes in the transparent medium between the sensor and the surface would be tolerable only if they were homogeneous, or if their inhomogeneities were random functions of time. If a strain distribution were required, the loading would have to be repeated for each positioning of the strain sensor.

SECTION VI

OPTICAL STRAIN MEASUREMENT INVESTIGATIONS

During the course of the investigations the HOSS system was applied to the measurement of strain on both a simple beam and a turbine engine blade. In both cases, both static and vibratory strain measurement were studied. Finally, experimental tests were also performed to evaluate the feasibility of applying the HOSS system to the detection of cracks in metals.

Strain Measurement on a Beam

Static Loading

Between twenty and thirty experiments were performed covering various aspects of the comparison of optical strain measurement to strain gage readout and to the analytically predicted strain in the sample. Some discussion of the apparatus is necessary to understand the discussion of the experimental results. Figure 18 is a diagrammatic sketch of the experimental apparatus assembled for the beam bending tests. (For clarity, the rod fixtures and connecting yoke have been omitted from the top view.) A and A' are rods against which the beam to be bent (shown shaded) is pressed. B and B' are rods that pivot about A and A'. C is a beam that receives force from a screw and transfers it to B and B'. The side view illustration shows the rod holding fixtures and the connecting yoke to the screw, while the front view of the apparatus shows the two strain gages positioned above and below the center line of the beam. The optical strain measurements were made in the center of the beam between the two strain gages. A dial was fastened to the back of the yoke, centered on the screw hole, and a pointed indicator fastened to the screw. This gave an accurate indication of the displacements of the rods B and bar C.

Some of the problems identified with the strain gages in these experiments were :

1. "Working-in" of the gage; the strain readings obtained on the first cycle of loading of the object may differ from subsequent cycles. Generally the strain readings dropped with cycling, often as much as five percent.

2. Prestressing of gages; some gages exhibited up to a negative 3500 microstrain after mounting on the sample.

3. Variations in hystersis; some gages would show hysteresis as the load on the bar was cycled while the companion gage would not.

Comments from the technical staff of the strain gage supplier (MicroMeasurements, Inc.) were that these problems related to the adhesive used.

FIG. 18

BEAM BENDING APPARATUS

(TOP)

(FRONT)

(SIDE)

38
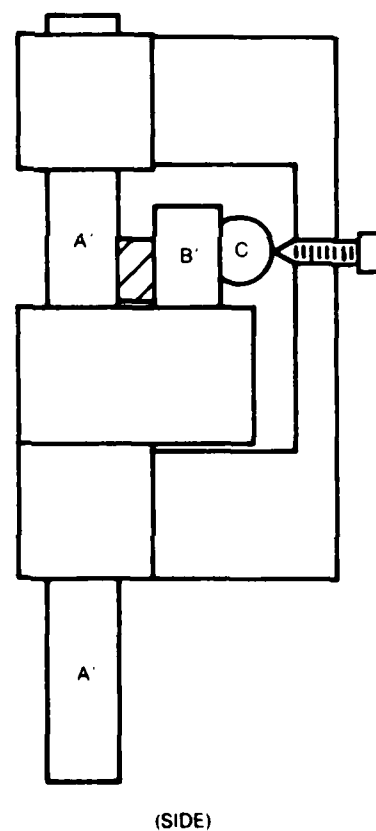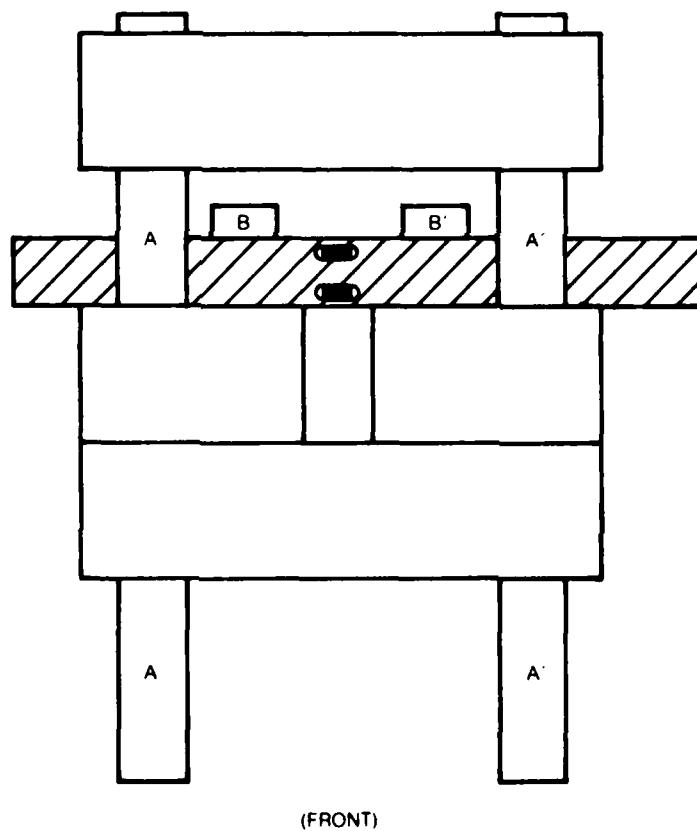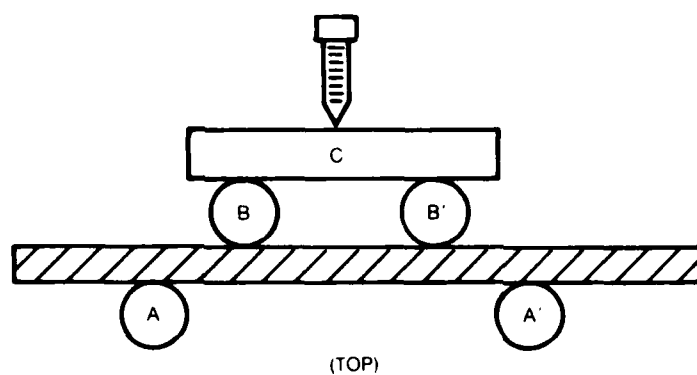
In order to determine the actual hysteresis of the beam during the load cycle, the following experiment was performed. A small mirror was cemented to the end of the bar, and a laser beam was reflected from the mirror and brought to a focus with a 400 mm focal length lens. The deflection of the focal spot could be accurately measured by a knife edge on a translation stage and this distance was directly related to the angular rotation of the end of the beam. Subsequent analysis of the general equations for the bending of a beam showed that for a beam under four point bending, the strain at the center of the beam, ϵ, is related to the rotation of the end of the beam, ω, by

$$\epsilon = T\omega/x , \tag{7}$$

where T is the beam thickness and x is the distance between the midpoints of the pairs of opposed forces (i.e., A and B and A' and B' in Fig. 18). This relationship is independent of shear in the beam, and therefore provides a very accurate way of measuring the strain in a bent beam. It was estimated, from the accuracy of the knife edge measurement, that the strain, analytically calculated in this manner, could be determined to within ±3 microstrain.

Figure 19 shows a set of results comparing two strain gage readings on a single beam to corresponding analytical strain calculations from mirror rotations at the end of the beam. The strain is plotted versus the angle through which an 8 x 32 screw, that bends the beam, has been turned. (The results for the lower gage have been displaced sideways from those of the upper gage to avoid confusing the plotted curves.) It can be seen that the readings from the lower gage agree well with the analytical calculations, including the correct hysteresis, whereas those from the upper gage do not. These results are representative of other similar experiments.

The results from the lower strain gage on the beam, as shown in Fig. 19, provided a good comparison to the strains measured by the optical strain sensor, and by the mirror rotations. Some modifications were made to the loading fixture that reduced the hysteresis of the system considerably (mostly more freedom of movement to the rods B and B'). These results are presented in Fig. 20, where the optical and strain gage readings are plotted versus the strains calculated from the mirror rotations. (The logarithmic scales allow percentage errors to appear as constant deviations above or below the line at 45° to the axes.)

The circles are data from the strain gage readings, and the squares are data from the optical strain sensor. The arrows denote load being applied when they point upward and load being removed when pointing downward. The solid line corresponds to exact agreement with the analytical calculations, based upon the mirror rotations. This data indicates a similar level of performance between the strain gage and the optical strain sensor. Resetting of the optical sensor to a new location is facilitated by the in-situ recording system for the photographic plates, and cycling time is between five and ten minutes. This is considerably less time than is required for reapplication of a strain gage.
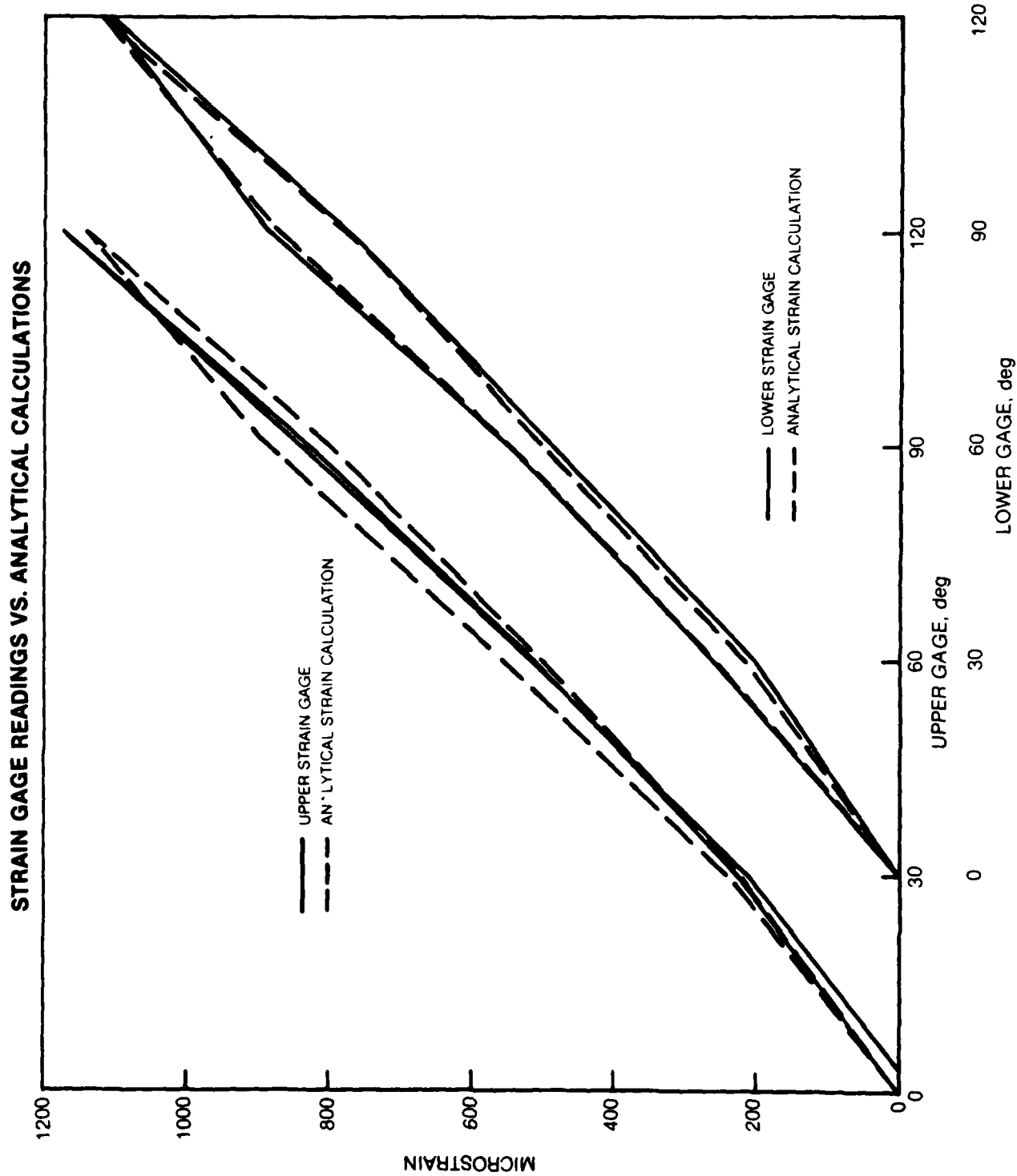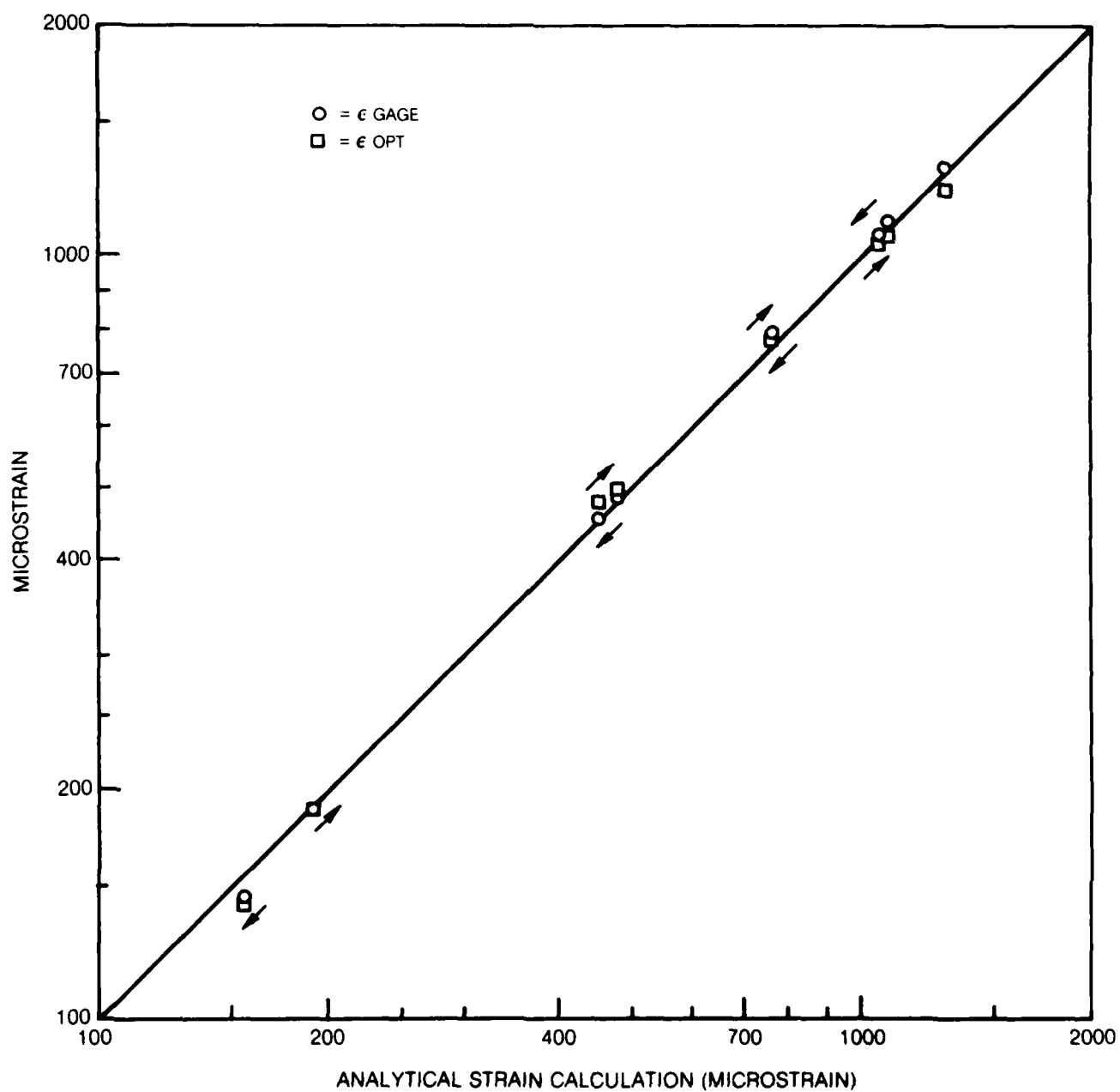
FIG. 19

STRAIN GAGE READINGS VS. ANALYTICAL CALCULATIONS

40

ANALYTICAL STRAIN CALCULATION VS. OPTICAL STRAIN SENSOR VS.
STRAIN GAGE MEASUREMENTS

Dynamic Loading

For the vibratory strain measurement tests, two objects (schematically illustrated in Fig. 21) were fabricated to provide vibration characteristics free of rotation that could affect the measurement of strain. (When strain is accompanied by an angular deviation of the surface, it results in a loss of signal strength as the strain level increases.) The first object (Fig. 21a) was a double-ended tuning fork with a mounting fixture at its center. With this object excited at resonance, the vibrations of one pair of tines are balanced by counter vibrations of the other pair, and vibrations at the center of either side will have, theoretically, no angular deviation. The second object (Fig. 21b) was a conventional tuning fork having sufficiently long tines (5.25 inches) to allow excitation of the second mode of the fork at a usable frequency (1441 Hz). The vibration at the antinode of either tine of this tuning fork (indicated by P) would also, theoretically, not exhibit angular deviation.

When these objects were examined, using the HOSS system, at the region where the angular deviations should be zero, it was found that the signals from the two detector channels were not purely in- or out-of-phase, as would be expected for a single mode of vibration. Plotted in Fig. 22 are the ratio of the two signal magnitudes (top) and the phase difference between the two channel signals (bottom) as a function of position along the tine of the conventional tuning fork (Fig. 21b). The data was taken at 5 mil increments over a region that included the antinode of vibration (P). Included with the data points (dots) are plots (solid lines) of the hypothetical outputs based upon a theoretical model of the object motion. The model used assumed that the vibratory bending (composed of the strain and spatially variant rotation) was accompanied by a uniform rotation of the surface which is both: 1) in phase quadrature with the strain related vibration (vibratory bending); and 2) of sufficient magnitude to generate a signal equal in magnitude to that due to the strain. The equations used were:

$$\tilde{A} = \phi_I \exp(i\pi/2) + \phi_R x - \epsilon, \text{ and}$$

$$\tilde{B} = \phi_I \exp(i\pi/2) + \phi_R x + \epsilon,$$

where

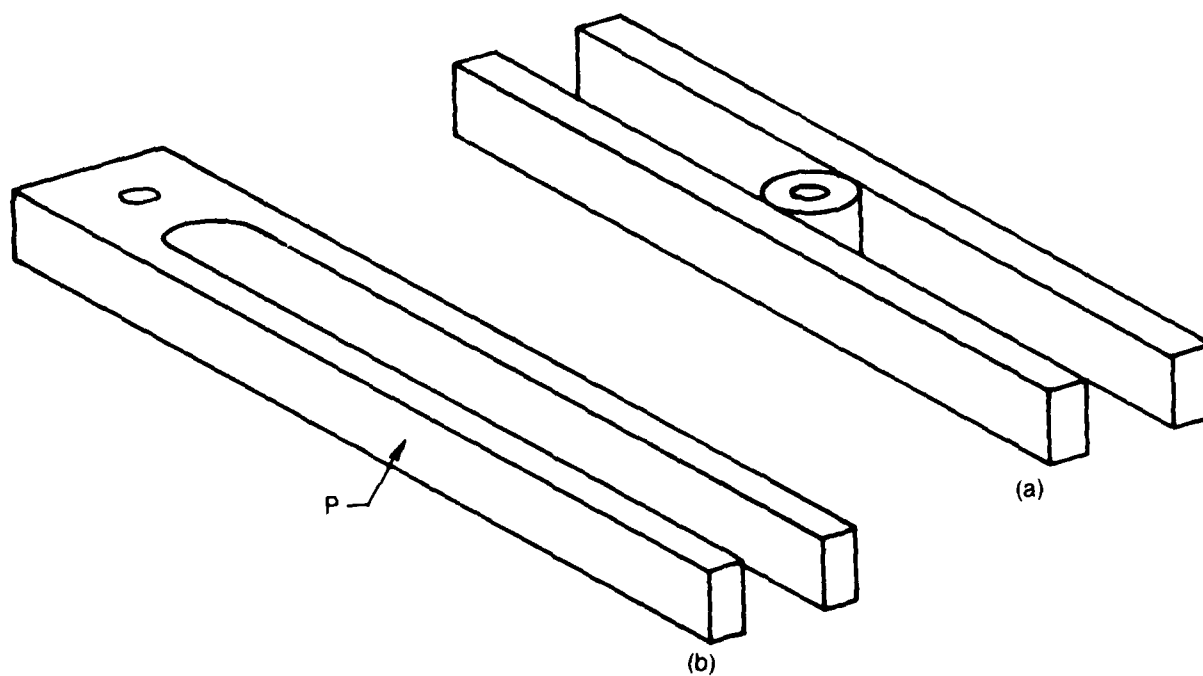$\tilde{A}$ and $\tilde{B}$ are the complex signal amplitudes from the two detector channels,

ϕ_I is the uniform quadrature rotation,

ϕ_R is the spatially variant rotation, and

ϵ is the strain

42

FIG. 21

TUNING FORK TEST OBJECTS

P

(a)

(b)

When the data was taken, the signal magnitudes were measured by the method of counting zero-crossings, and the phase was measured using a phase meter with the heterodyne generator stationary and oriented for best signal quality.

The agreement between the data and the model, as shown in Fig. 22, is sufficient to justify the use of this model in data processing. The physical mechanism responsible for this behavior would appear to be a coupled response between the fundamental mode of the tuning fork, some other mode of the fork, and possibly the mounting structure. The response did not appear to be a linear superposition of independent vibration modes which is most often the source of a complex vibratory response for the following reasons: 1) the phase relationship between the two signals was observed to vary only slightly, if at all, as the excitation frequency was tuned through resonance; and 2) the phase relationship appeared to be relatively uninfluenced by changes in the effective position of excitation. (These two effects have been used extensively in holographic vibration analysis to identify linear mode combinations and to adjust excitations for single mode response.)

Because of the considerable difficulty encountered in trying to eliminate this complex response, a method had to be devised to deal with it. The strain components can be obtained from the above equations if the two are subtracted as phase vectors. Because the phase difference between the two signals was independent of signal amplitude, this parameter could be measured once (at an appropriate signal amplitude) and then used for a variety of measurements at different levels of excitation. At each excitation level, the magnitude of both signals A and B would be measured, the phase difference assigned to one of them, and then the two subtracted as phase vectors. These computations are easily performed on a programmable calculator.

To experimentally evaluate this technique, the double-ended tuning fork (Fig. 21a) was strain gaged at the middle of one side, above and below the center. Magnetic patches were cemented near the ends of the tines, and electro-magnet exciters placed near those patches at the ends of the tine being observed. An optical vibration pickup was placed near one end of the other tine and connected through a band-pass filter and signal limiter to the drive amplifier for the exciters. In this manner, stable, self-sustaining oscillations were provided at the natural frequency of oscillation of the object. The strain gages were read using a Tektronix oscilloscope with a type Q plug-in module. The phase difference between the two channels was measured with a convenient signal amplitude and stored.

Different strain levels, ranging from 100 microstrain to 2000 microstrain, were set by the strain gage readout. At each level, three measurements of the signal magnitude were taken for each channel and used to compute three values of

44

FIG. 22

**RATIO OF SIGNAL MAGNITUDES AND PHASE DIFFERENCE BETWEEN SIGNALS**
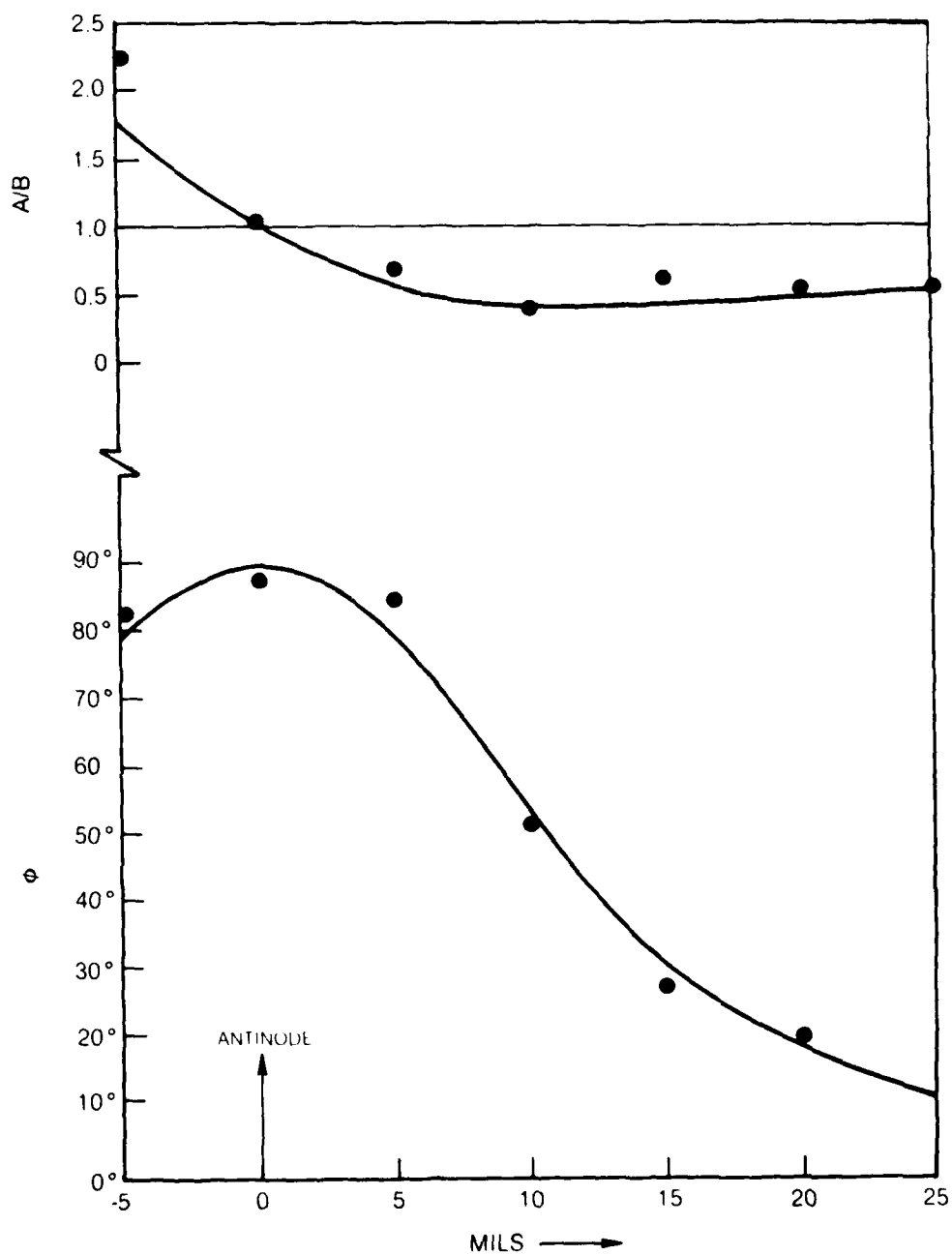
the optically measured strain. The three measurements were averaged and the standard deviation computed; the latter was consistently on the order of ± 0.5 percent. A plot of the optical strain versus the gage strain is presented in Fig. 23 on a logarithmic scale. The straight line at 45 degrees corresponds to perfect agreement between the two. The optical strain measurements at the vibration node are in excellent agreement with the strain gage data from 600 to 2000 microstrain, but are slightly higher at the lower strain values. The error, which is approximately 30 microstrain, may be assigned to the noise generated by various random vibrations on the table. The minimum detectable strain, calculated by taking the ratio of the heterodyne frequency to the vibration frequency, is about 70 microstrain.

Tests were then run to determine the effect of location of the strain measurement on the accuracy of the data. Optical strain measurements were made at four locations on the four-tined fork: at the vibration node and 0.63 mm (25 mils), 1.27 mm (50 mils), and 1.90 mm (75 mils) to the right of the vibration node. Figure 24 presents a plot of the errors between the optical strain measurement and the resistive strain gage data as a function of the values read from the resistive gage. (Two independent measurements were made at the 50 mil location.) The cross hatched area in the lowest plot shows the band that corresponds to ± 2 percent error. What is noticable in these plots is that the maximum strain that can be measured drops sharply as the measurement point shifts away from the node line. This results from the increase in surface tilt that accompanies the vibratory strain which increases the number of phase cycles that are associated with each vibation cycle. The primary effect of this increase in surface tilt is to increase the bandwidth of the signals, and it has been determined that the electronics of the detectors show a fall-off in gain beyond about 2000 Hertz.

Four of the measurements (lower section of Fig. 24) were made with a 1 mm spot separation of the illuminated regions of the object. An additional measurement was made at the node line with a 2 mm spot separation; this is shown at the top of Fig. 24. The increase in spot separation has the effect of doubling the signal to noise ratio and thereby halving the minimum detectable strain. With this spot separation, the system still performs well up to 2000 microstrain.

Strain Measurement on a Turbine Blade

For this phase of the investigation, a representative turbine blade was mounted in a broach block, as illustrated in Fig. 25, and clamped by a suitable fixture until rigid. The entire assembly was fastened to an x,y translation stage with the span of the blade horizontal; by raising and lowering the assembly, different blade spans could be studied. For static deflections, a pair of side flanges were bolted to the clamping fixture which supported a cross beam through which a screw was threaded to press laterally against the blade tip, as illustrated in Fig. 26. For the vibratory studies, a heavy duty shaker was bolted in contact to the clamping fixture through the vertical rod shown to the right of the blade in Fig. 27.
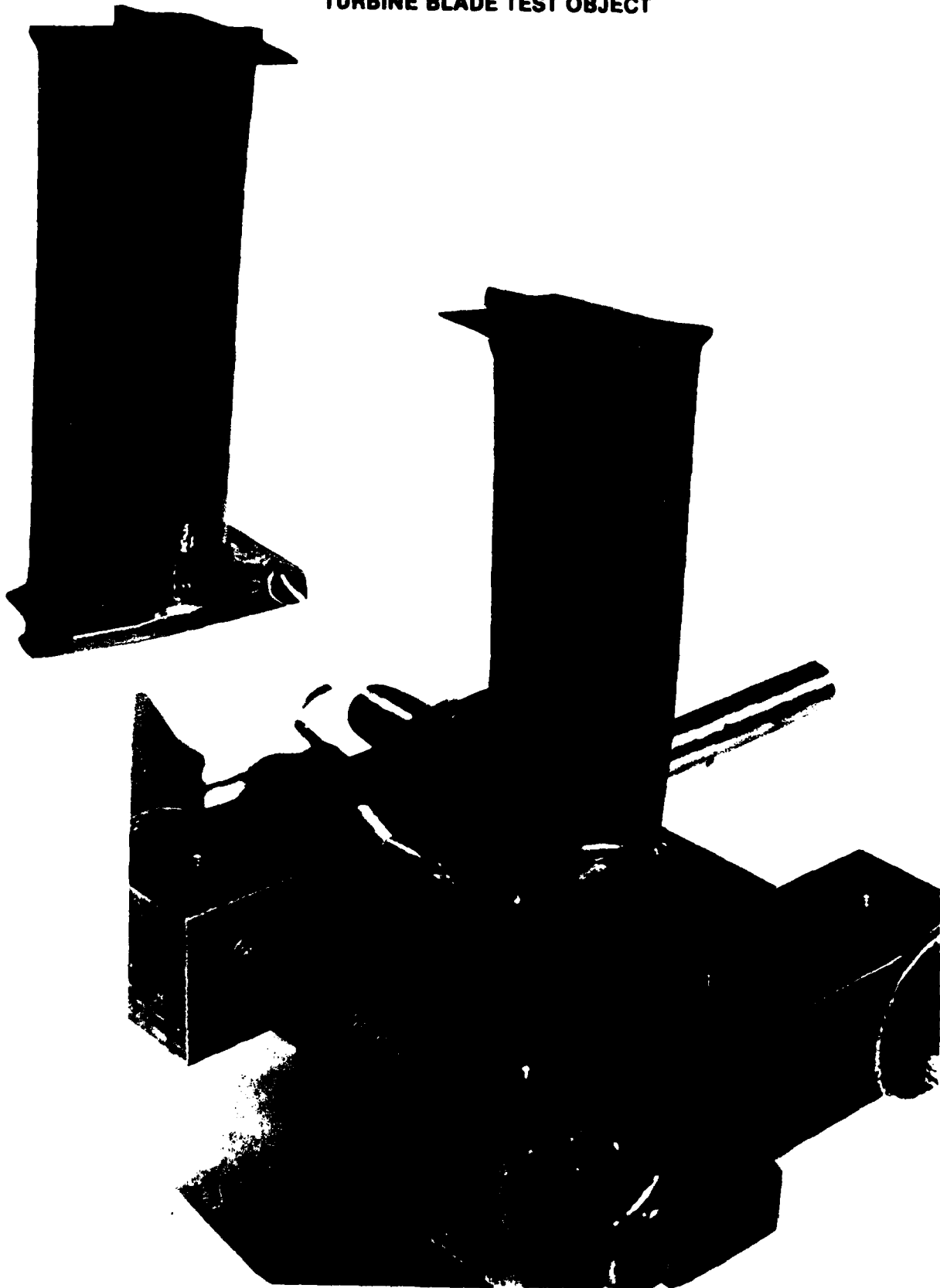
FIG. 23

OPTICAL STRAIN SENSOR vs STRAIN GAGE MEASUREMENT

FIG. 24
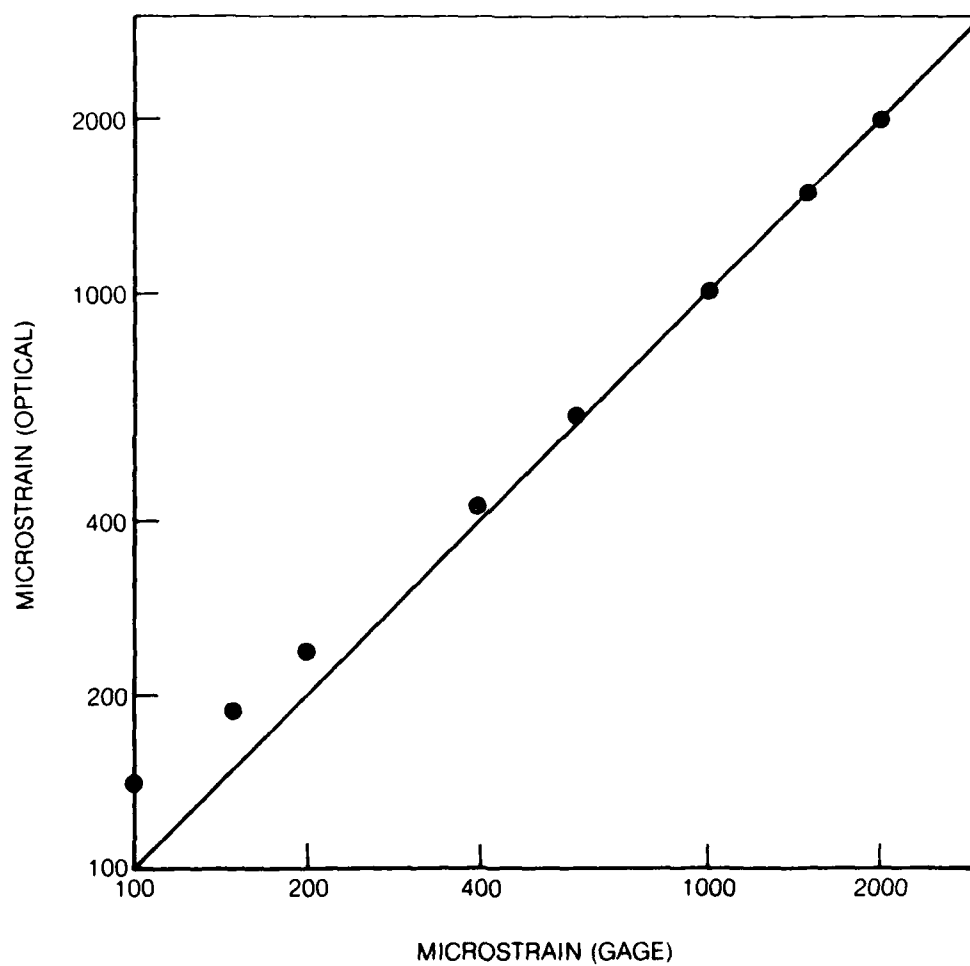
EXPERIMENTAL ERROR AS A FUNCTION OF GAGE VALUE, DISTANCE FROM VIBRATION NODE (D) AND SPOT SEPARATION (ΔX)
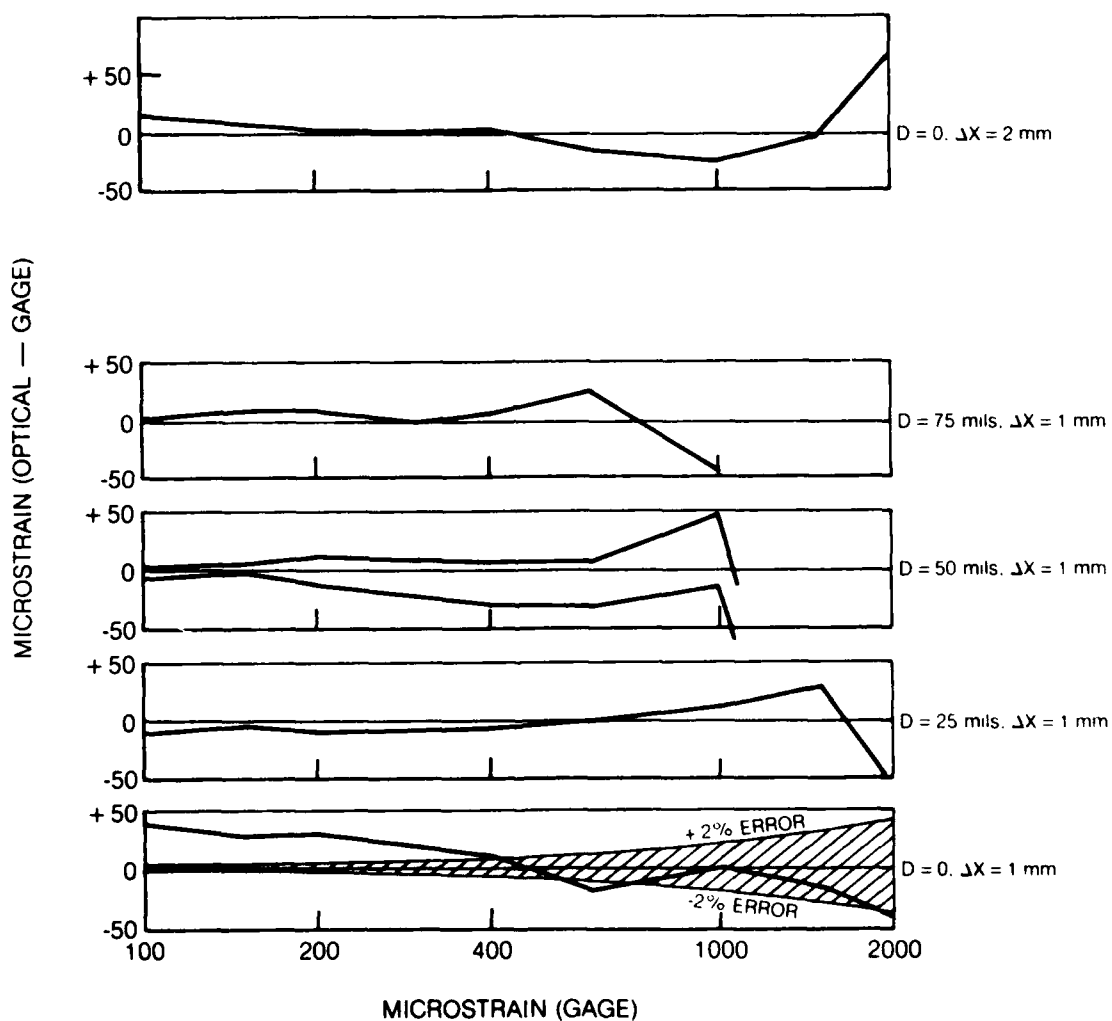
FIG. 25

TURBINE BLADE TEST OBJECT
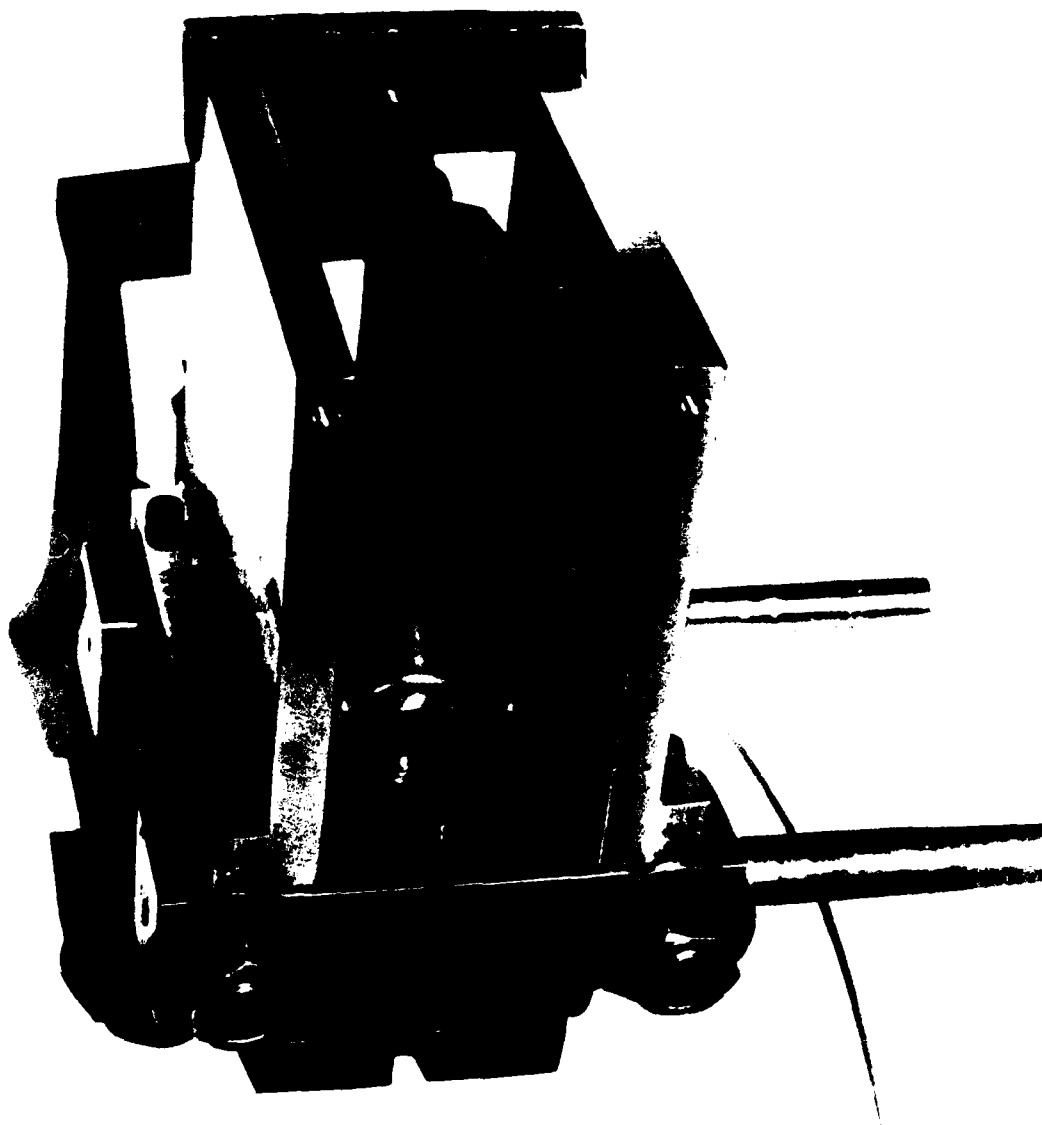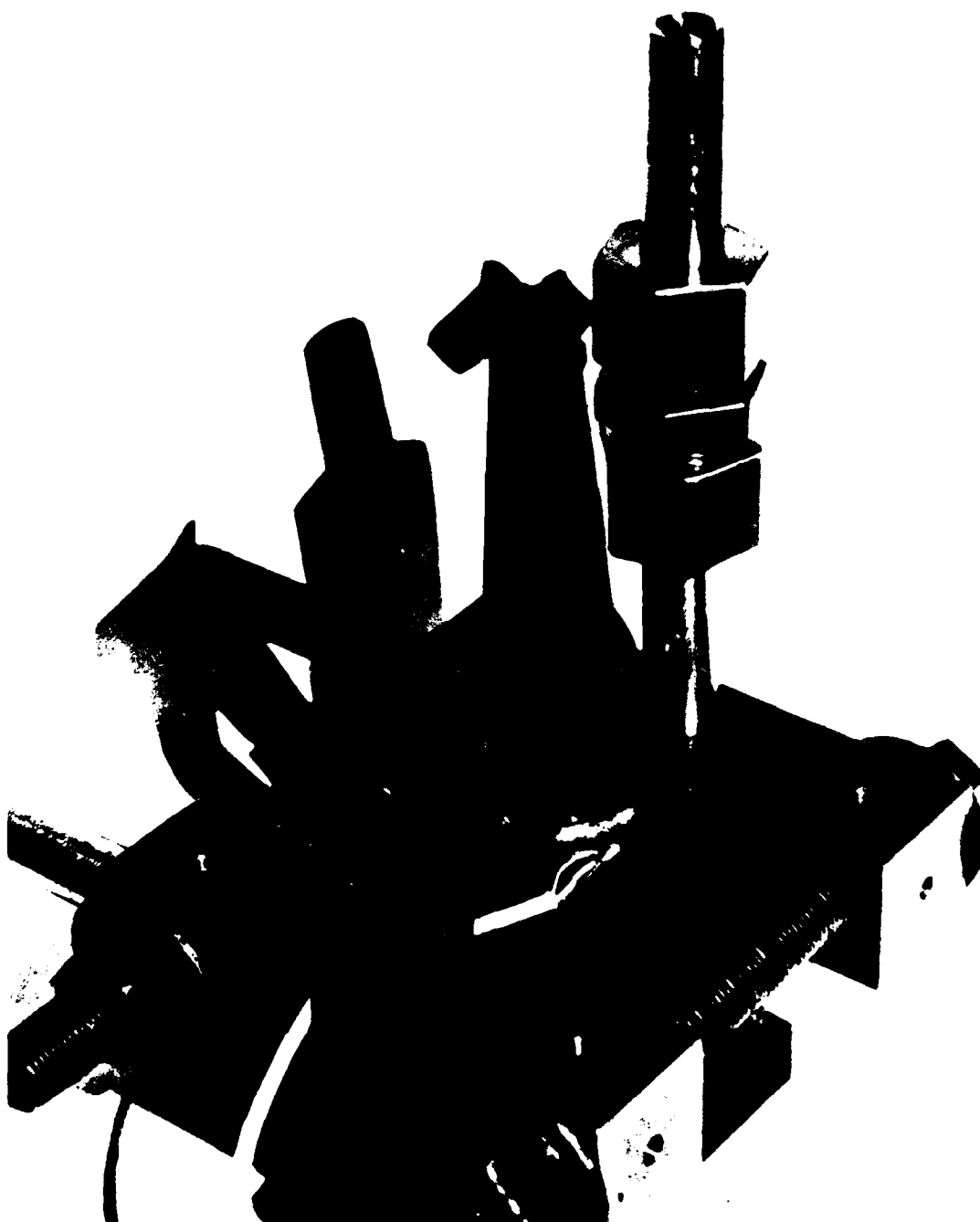
FIG 26

STATIC STRESSING ASSEMBLY

FIG 26

FIG. 27

DYNAMIC STRESSING ASSEMBLY

FIG. 27

Optical Alignment Procedure

In order to measure surface strains correctly, the optical strain sensor must be oriented along the normal of the surface under study. Determination of this can be a problem when the surface is highly curved such as that of a turbine blade. Two techniques were used for this purpose in the present study. The first and simplest was to observe the two illuminated spots on the object from an angle of about 45° to the horizontal in a plane parallel to the illumination. If the surface is tilted about a vertical axis relative to the illumination direction, then one spot will appear to be behind the other. The object may then be rotated in a horizontal plane until both spots appear to be the same distance from the strain sensor. Although the surface may still be tilted to the illumination about a horizontal axis, this tilt will not affect the strain reading.

The second technique used, was to observe the light reflected or scattered back toward the source of illumination. A slight polishing of the metal surface of the turbine blade, enough to make it shiny, would enhance the specular reflectance to the point where it could be observed and centered on the illumination beams. Rubbing the surface with oil would also help accomplish the same thing. This technique was employed only when complete alignment with the surface normal was sought.

These two techniques were sufficient to align the surface to within approximately 5 degrees of normal illumination. This would reduce the admixture of surface rotations into the strain measurement to less than ten percent. It was not a difficult matter to make these adjustments even on highly curved surfaces such as the leading and trailing edges and the root fillets.
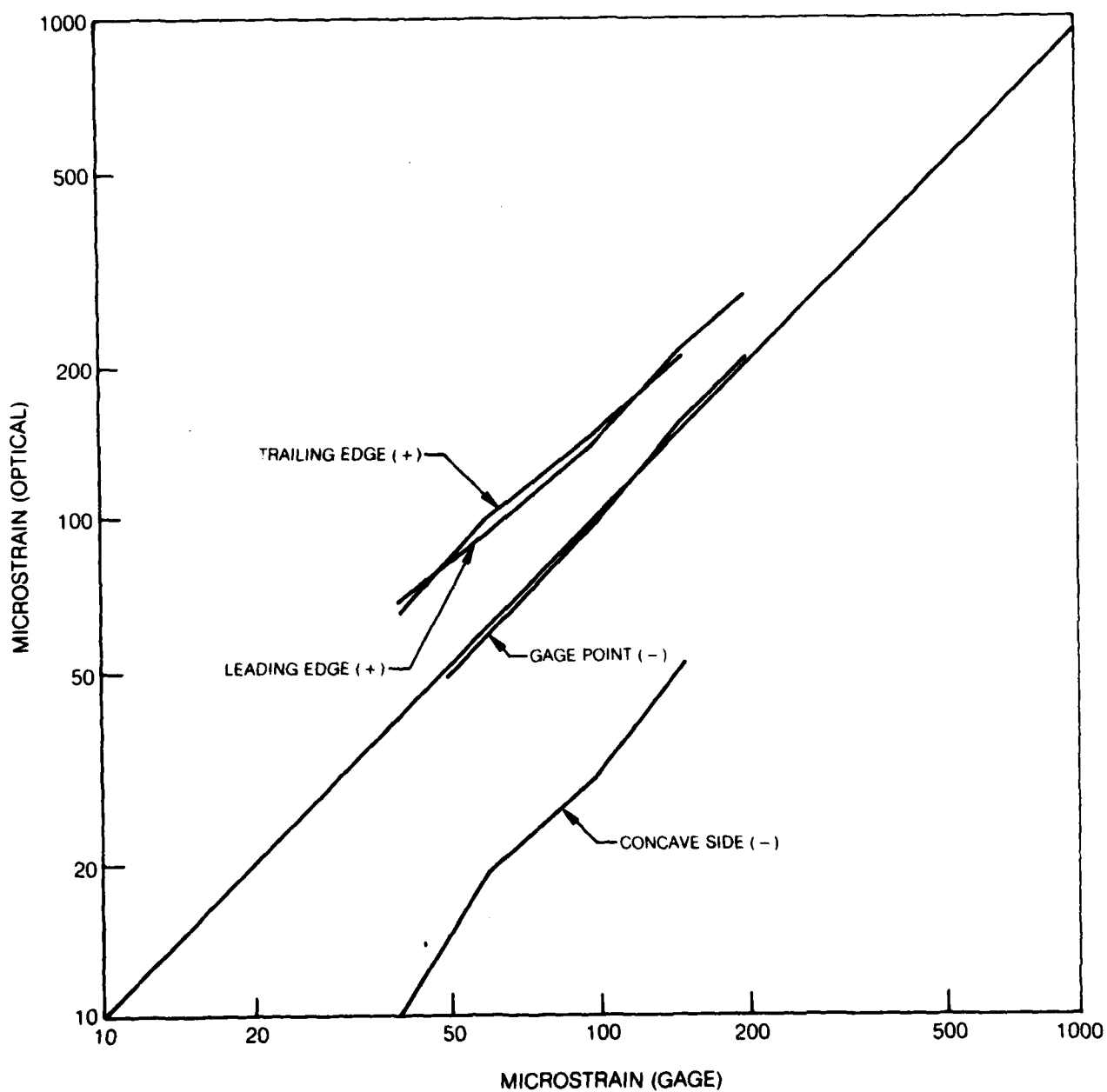
Static Loading

With a bending deflection applied to the tip, as described above (Fig. 26), static strain measurements were made at four locations along a chord 10 mm above the root of the turbine blade: just above the gage point; at the leading edge; at the trailing edge; and in the concave region of the blade (see Fig. 28). The results obtained in these studies are plotted in Fig. 29, with the values obtained just above the gage point seen to be in good agreement with the gage readings. The optical measurements at the leading and trailing edges were approximately 1.5 times those at the gage point and were of the opposite sign, whereas, those obtained in the concave region of the blade were only about 0.3 times the gage point readings and were of the same sign. The reversal of strain direction between the edges and the concave region of the blade indicates that the neutral surface, not surprisingly, lies outside the blade for a portion of its cross section. Strains much above 200 microstrain could not be measured due to the loss in signal caused by angular deviation of the blade under bending. (Though of a different scale, this problem was alluded to earlier with typical results plotted in Fig. 12.)

FIG. 28

STRAIN MEASUREMENT LOCATIONS

FIG. 29
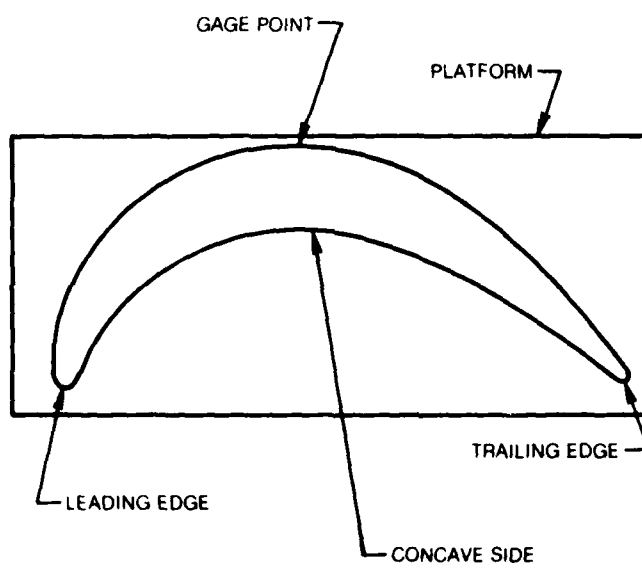
OPTICAL STRAIN SENSOR vs STRAIN GAGE MEASURMENT
**STATIC STRESSING OF TURBINE BLADE**

54

Dynamic Loading

Several attempts were made to measure the vibratory strain with the
blade excited in its fundamental resonance at 1247 Hz. Whereas some results
obtained at the leading edge did agree approximately with the static strain data,
the results obtained at the trailing edge, and at the gage location, did not.
The loss of signal due to the angular displacement was so severe that the reli-
ability of the results was poor. Attempts were made to obtain the vibratory
strain in the fillets of the leading and trailing edges, but the angular displace-
ments were still too great.

Crack Detection in Metals

As a part of the investigation, a preliminary study was performed to examine
whether the HOSS system would be capable of detecting cracks. A small notch was
formed in the center of a beam of aluminum by pressing a rounded exacto knife
into the surface. The simulated crack was about 5 mm long and about 0.2 mm deep.
The aluminum beam was placed in the fixture for four-point bending, which was
mounted on a translation stage. Strain measurements were then made versus
load-point deflection for each of three locations on the beam: one where both
spots were to the right of the crack; one where the spots were to either side of
the crack; and one where both were to the left. These locations are shown in
Fig. 30, and are labeled 1, 2, and 3 respectively. The strains obtained for a
0.2 mm deflection of the load point were 747$\mu\epsilon$, 880$\mu\epsilon$, and 790$\mu\epsilon$, for points 1,
2, and 3 respectively. The indicated strain for the measurement where the crack
was between the two illuminated spots was 14.5 percent above the average of the
measurements to either side. This is considered to be a dramatic indication of
presence of a crack that is, itself, only 4 percent of the beam thickness in
depth. This increase in strain corresponded to about a 20° change in phase
difference between the two detector signals. The amount of perturbation that
this would generate in holographic fringes would be virtually unnoticable. The
conclusion is that the heterodyne optical strain sensor should be very effective
for crack detection.

55

FIG. 30

CRACK DETECTION BY STRAIN MEASUREMENT

NO. 2

NO. 1

CRACK

NO. 3
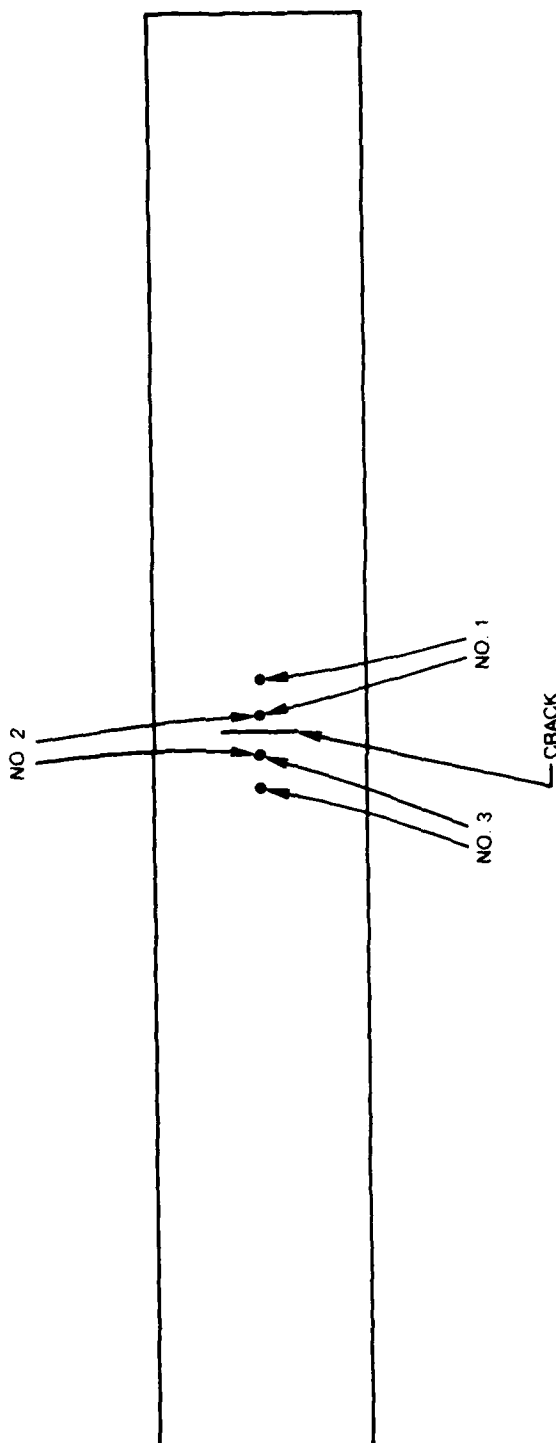
SECTION VII

CONCLUSIONS AND RECOMMENDATIONS

Under the present contract, the heterodyne optical strain sensor was shown to provide strain indications with an accuracy comparable to that of a properly bonded train gage. The significant results from the investigations can be enumerated as follows:

1. The HOSS system can measure static strains with a sensitivity approaching one microstrain and an accuracy approaching one percent, to a range of ± 2000 microstrain.

2. The HOSS system can measure vibratory strains with the same sensitivity and accuracy to a range of 2000 microstrain peak-to-peak.

3. Insensitivity to object translations is achieved by proper spacing between the transform lenses and the recording plane; this is an initial adjustment that could be preset.

4. Both static and vibratory strain measurement are limited in practice by surface tilt (or rotation); however, the vibratory measurements are much more severely limited.

5. Sensitivity to ambient noise is greater for vibratory strain measurement due to a lack of signal filtering.

6. In-situ photographic processing permits a far more rapid relocation time (5 to 6 minutes) than is possible with strain gages, whose adhesive curing time is measured in hours if force is to be accurately transmitted from the object surface to the gage; however, a more rapid in-situ recording and detection scheme (on the order of 15 seconds) would be preferred.

7. The HOSS system can be used effectively to measure static strains on actual jet engine turbine blades and other components to within the limits set by concomitant surface tilt.

8. The HOSS system is applicable to highly curved surfaces, such as turbine blade fillets, provided optical access in available; however, a six-degree-of-freedom positioner would be desirable for alignment of the part under study relative to the strain sensor.

9. The HOSS system appears to be very effective for crack detection in metals by virtue of the crack-related discontinuity in a strain vs. position plot across an object surface.

The above enumerated results taken as a whole represent the second major advance in the field of optical strain measurement that has come about with the introduction of optical heterodyning techniques into the field of optical metrology; namely, the real-time, point measurement of strain with accuracy and sensitivity comparable to electrical strain gages. The first, also reported by UTRC as recently as 1980 (Ref. 3), allows the high precision, post-test (non real-time) measurement of strain distributions on objects that may be subjected to non-repeatable stress cycles, such as those due to thermal stressing. In practice, data is taken as a set of single-exposure speckle photographs (specklegrams) which are recorded at discrete time intervals and subsequently processed via heterodyne readout of the halo fringes from specklegram pairs to extract strain data. This technique of applying heterodyne interferometry to specklegram halos (or HISH) can also tolerate up to approximately 10 milliradians of surface tilt without degradation of the results; an order of magnitude better than the HOSS system.

Relevant to general-purpose strain measurement, a combination of the preferred features of both the HOSS and HISH systems would permit the real-time strain mapping of an object under a single loading condition with immunity to surface tilt. It is felt that the introduction of heterodyne readout into a conventional experimental approach to speckle interferometry, as suggested by Leendertz in his original publication (Ref. 6) in the field, should permit just such a measurement. Consequently, an investigation of the heterodyne interferometry of speckle correlation (or HISC), as described below, is recommended for investigation.

Experimentally, the object would be illuminated by two mutually coherent beams of laser light that make equal but opposite angles to the surface normal. A camera would be located with its optical axis along the surface normal and a photographic transparency recorded, developed, and relocated in the original image plane. The speckles formed at the image plane by the interference of the two fields scattered by the object surface will be blocked by the corresponding opaque portions of the transparency, and this will give a null in the amount of light transmitted through the recording. If the relative phase of the two interfering fields is changed by 180°, the resulting speckle pattern will have no correlation with the pattern of the recording and a maximum of light will be transmitted. If the phase is continuously varied, the correlation of the pattern in the incident field with the pattern of the recording will vary cyclicly, as will the amount of transmitted light.

The phase change between the two scattered fields could be generated in either of two ways. First, it could be generated by a displacement of the object parallel to the difference of the propagation vectors of the two illumination beams. Second, it could be generated by introducing a heterodyne frequency shift between the two illumination beams. If a heterodyne frequency shift is used to generate the fluctuating light intensity transmitted through the recording, then static transverse object displacements would show up as constant changes in the

58

phase of the output light fluctuations. These phase changes could be measured very accurately by detecting the output light fluctuations with a photoelectric sensor and feeding the signal into an electronic phase meter. If object displacements are to be measured, a single detector would be required and the phase changes would be measured relative to the heterodyne generator signal. If spatial variations in displacement are to be measured (which may be related to strain), then two detectors would be used and the phase difference between the two signals measured.

This system would allow the measurement of strain distributions under a single loading condition because the initial recording would preserve information about the object surface over an area, rather than at a single pair of points. If the difference of the propagation vectors of the two illumination beams lies in the object surface, then surface tilts would not generate phase changes in the output signals because the corresponding surface displacements would lie out of the surface.

For reference, the operational characteristics of the three heterodyne systems:

1. Heterodyne Optical Strain Sensor - HOSS (current contract and Ref. 7)

2. Heterodyne Interferometry of Specklegram Halos - HISH (Ref. 3), and

3. Heterodyne Interferometry of Speckle Correlation - HISC (recommended for study),

are summarized in Table I.

It can be concluded that the development of optical heterodyning techniques, in combination with speckle metrological technology, should be continued because of the extraordinary promise they hold for the future of strain measurement. Such devices, potentially capable of submicrostrain resolution up to several thousand microstrain, would not only compete with resistive strain gages, but should out perform them in numerous applications, while maintaining their distinct, non-contact advantage.

TABLE 1

Heterodyne Strain Sensing Systems Characteristics

	HETERODYNE OPTICAL STRAIN SENSOR -HOSS-	HETERODYNE INTERFEROMETRY OF SPECKLE CORRELATION -HISC-	HETERODYNE INTERFEROMETRY OF SPECKLEGRAM HALOS -HISH-
Temporal Data Base	← Real Time →		Time Delay (Stored)
Spatial Data Base	Uniaxial Strain at One Location	Uniaxial Strain Distributions by Scanning or by Multi-Channel Output	Rosette Strain Distributions by Scanning
Strain Sensitivity (Based on λ/1000)	~ 1 με at 1 mm and $\pm14^{o}$ (Function of Beam Separation and Viewing Angles)	~ 1 με at 1 mm and $\pm14^{o}$ (Function of Detector Spacing and Illumination Angles)	5 με at f/10 (Function of f-number)
Calibration Accuracy	~ 1%	~ 1% (Dependent upon Accuracies in Measuring Distances and Angles)	~ 1%
Light Required	← Laser Exposure → ← Laser Readout →	Laser Exposure Laser Readout	Laser or White Light Exposure Laser Readout
Vibration Measurement	Easily Modified via Readout Logic		Difficult to Do Careful Exposure Timing Required
Limitations on – Axial Displacement	Several Millimeters	~ 4 λ $(f\text{-no.})^2 \approx 0.2$ mm at f/10 (Set by Speckle Decorrelation Due to "Depth of Focus")	
– Lateral Displacement	~ $\pm$ 0.05 mm (Function of Spot Size) (Object Tracking Possible)	~ λ (f-no.) ≈ 0.006 mm at f/10 (Function of Speckle Size) (Object Tracking Possible)	Virtually No Limit Due to Realignment in Readout
– Surface Tilt	~ 1 milliradian for 100 μm Spot Size (Limited by Transform Plane Translation)	~ 10 milliradians for f/10 → (Limited by Speckle Decorrelation Due to Translation of Field at Lens Aperture)	
–To avoid Degradation in the Measurement			

60

REFERENCES

1. Stetson, K. A. and I. R. Harrison: Optical Heterodyne Strain Sensor. UTRC Patent Disclosure dated March 3, 1980.

2. Dandliker, R. and B. Eliasson: The Accuracy of Heterodyne Holographic Strain and Stress Determination. Experimental Mechanics, 19, 93-101 (March 1979).

3. Smith, G. B. and K. A. Stetson: Heterodyne Readout of Specklegram Halo Interference Fringes. Applied Optics, 19, 3031-3033 (September 15, 1980).

4. Stetson, K. A.: Use of Projected Matrices in Hologram Interferometry. Journ. Opt. Soc. Amer., 69, 1705-1710 (1979).

5. Shumann, W. and M. Dubas: Holographic Interferometry, Springer-Verlag, Berlin, Heidelberg and New York, 1979, p. 14.

6. Leendertz, J. A.: Interferometric Displacement of Scattering Surfaces Utilizing Speckle Effect. J. Phys. E., Sci. Instrum.. 3, 214-218 (1970).

7. Stetson, K. A.: Strain Measurement on Rough Surfaces by Optical Heterodyning. Proceedings of the 1981 Spring Meeting of SESA, 236-241 (1981).